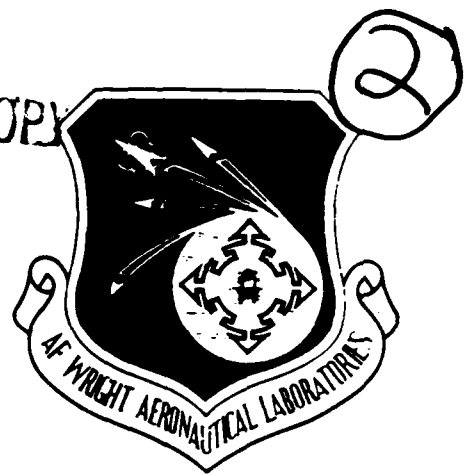


DTIC FILE COPY



AFWAL-TR-87-3022

STRESS INTENSITY FACTORS FOR CRACKING METAL STRUCTURES UNDER
RAPID THERMAL LOADING

An-Yu Kuo
P. C. Riccardella

Structural Integrity Associates
San Jose, CA 95118

Joseph P. Gallagher

University of Dayton Research Institute
Dayton, OH

June 1987

Final Report for Period July 1986 - February 1987

Approved for public release; distribution unlimited.

FLIGHT DYNAMICS LABORATORY
AIR FORCE WRIGHT AERONAUTICAL LABORATORIES
AIR FORCE SYSTEMS COMMAND
WRIGHT-PATTERSON AIR FORCE BASE, OHIO 45433-6553

DTIC
ELECTE
AUG 27 1987
S D

87 8 26 037

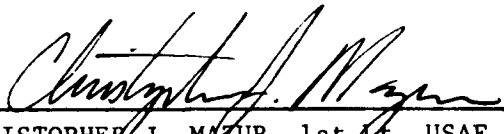
AD-A184 112

NOTICE

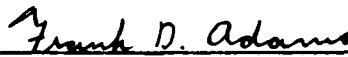
When Government drawings, specifications, or other data are used for any purpose other than in connection with a definitely related Government procurement operation, the United States Government thereby incurs no responsibility nor any obligation whatsoever; and the fact that the government may have formulated, furnished, or in any way supplied the said drawings, specifications, or other data, is not to be regarded by implication or otherwise as in any manner licensing the holder or any other person or corporation, or conveying any rights or permission to manufacture use, or sell any patented invention that may in any way be related thereto.

This report has been reviewed by the Office of Public Affairs (ASD/PA) and is releasable to the National Technical Information Service (NTIS). At NTIS, it will be available to the general public, including foreign nations.

This technical report has been reviewed and is approved for publication.

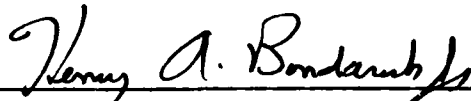


CHRISTOPHER J. MAZUR, 1st Lt, USAF
Fatigue, Fracture & Reliability Group
Structural Integrity Branch



FRANK D. ADAMS, Chief
Structural Integrity Branch
Structures Division

FOR THE COMMANDER



HENRY A. BONDARUK, JR, Colonel, USAF
Chief, Structures Division

"If your address has changed, if you wish to be removed from our mailing list, or if the addressee is no longer employed by your organization please notify AFWAL/FIBEC, W-PAFB, OH 45433 to help us maintain a current mailing list".

Copies of this report should not be returned unless return is required by security considerations, contractual obligations, or notice on a specific document.

A12112

REPORT DOCUMENTATION PAGE				Form Approved OMB No. 0704-0188	
1a. REPORT SECURITY CLASSIFICATION Unclassified			1b. RESTRICTIVE MARKINGS		
2a. SECURITY CLASSIFICATION AUTHORITY			3. DISTRIBUTION / AVAILABILITY OF REPORT Approved for public release; distribution unlimited		
2b. DECLASSIFICATION / DOWNGRADING SCHEDULE					
4. PERFORMING ORGANIZATION REPORT NUMBER(S) SIR-87-005			5. MONITORING ORGANIZATION REPORT NUMBER(S) AFWAL-TR-87-3022		
6a. NAME OF PERFORMING ORGANIZATION Structural Integrity Associates, Inc.		6b. OFFICE SYMBOL (if applicable)	7a. NAME OF MONITORING ORGANIZATION Flight Dynamics Laboratory (AFWAL/FIBEC) AF Wright Aeronautical Laboratories		
6c. ADDRESS (City, State, and ZIP Code) 3150 Almaden Expressway, Suite 226 San Jose, CA 95118			7b. ADDRESS (City, State, and ZIP Code) Wright-Patterson AFB, OH 45433-6553		
8a. NAME OF FUNDING / SPONSORING ORGANIZATION DOD SBIR Program Office		8b. OFFICE SYMBOL (if applicable)	9. PROCUREMENT INSTRUMENT IDENTIFICATION NUMBER F33615-86-C-3219		
8c. ADDRESS (City, State, and ZIP Code) Washington, DC 20301			10. SOURCE OF FUNDING NUMBERS		
			PROGRAM ELEMENT NO. 65502F	PROJECT NO. 3005	TASK NO. 30
11. TITLE (Include Security Classification) See Reverse					
12. PERSONAL AUTHOR(S) An-Yu Kuo, P. C. Riccardella, J. P. Gallagher					
13a. TYPE OF REPORT Final		13b. TIME COVERED FROM 0786 TO 0287		14. DATE OF REPORT (Year, Month, Day) 1987, June	
15. PAGE COUNT 88					
16. SUPPLEMENTARY NOTATION This is a Small Business Innovation Research Program, Phase I Report					
17. COSATI CODES			18. SUBJECT TERMS (Continue on reverse if necessary and identify by block number)		
FIELD	GROUP	SUB-GROUP	Stress Intensity Factors, Fracture Mechanics, Rapid Thermal Pulses, Crack Growth, Analysis		
13	13				
20	05				
19. ABSTRACT (Continue on reverse if necessary and identify by block number) An SBIR Phase I feasibility study has been conducted on a novel method of calculating cracktip stress intensity factors for cracked metal structures under rapid thermal pulse loadings. The work couples a Green's function integration technique for transient thermal stresses with the well-known influence function approach for calculating stress intensity factors. A preliminary version of a computer program implementing the methodology designated AF-CRACK, was developed and delivered with the Phase I project report. Operable on an IBM-pc or compatible, the program demonstrates the ability to accurately calculate stress intensity factors, with very short turnaround times, and immediate graphics visualization of the results. Based on the success of this Phase I feasibility study, it is highly feasible to develop a general purpose computer program based on this methodology, which is easy to use, fast, and accurate for predicting stress intensity factors (Continued on reverse)					
20. DISTRIBUTION / AVAILABILITY OF ABSTRACT <input type="checkbox"/> UNCLASSIFIED/UNLIMITED <input checked="" type="checkbox"/> SAME AS RPT <input type="checkbox"/> DTIC USERS			21. ABSTRACT SECURITY CLASSIFICATION Unclassified		
22a. NAME OF RESPONSIBLE INDIVIDUAL Lt. Christopher J. Mazur			22b. TELEPHONE (Include Area Code) (513) 255-6104		22c. OFFICE SYMBOL AFWAL/FIBEC

Unclassified

11. TITLE (Include Security Classification)

Stress Intensity Factors for Cracking Metal Structures Under Rapid Thermal Loading

19. ABSTRACT

for a wide range of metallic (or other) structures of interest to the Air Force, under rapid thermal pulses. It is also possible to connect the program with other fracture mechanics computer programs, in order to use the resulting stress intensity data in crack propagation or critical flaw size predictions.

The resulting AF-CRACK program would thus be expected to have extensive benefits and commercial applications to the Air Force and other organizations concerned with fracture mechanics and flaw tolerant design of airframe and other structures subjected to thermal transient loading conditions.

Accession For	
NTIS CRA&I	<input checked="checked" type="checkbox"/>
DTIC TAB	<input type="checkbox"/>
Unannounced	<input type="checkbox"/>
Justification	
By	
Distribution /	
Availability Codes	
Dist	Avail and/or Special
A-1	

QUALITY
INSPECTED
2

TABLE OF CONTENTS

<u>Section</u>	<u>Page</u>
1.0 INTRODUCTION AND PROBLEM STATEMENT	1
2.0 THEORETICAL SOLUTION	4
2.1 Assumptions	4
2.2 Governing Stresses	6
2.3 Stress Intensity Factor Influence Functions	6
2.4 Principle of Superposition	6
2.5 Green's Function for Time Integration . . .	7
2.6 Single Edge Cracked Plate and Center Cracked Plate	8
3.0 PHASE I DEMONSTRATION SOFTWARE (AF-CRACK) . . .	21
3.1 General Program Features	21
3.2 Software Architecture	21
3.3 Program Verification	26
4.0 SAMPLE PROBLEMS	39
4.1 Sample Problem 1 - Single Edge Cracked Plate	39
4.2 Sample Problem 2 - Center Cracked Plate .	40
5.0 CONCLUSIONS AND RECOMMENDATIONS	51
REFERENCES	54
 APPENDICES	
A - INFLUENCE FUNCTIONS	A1
B - SOLUTION FOR COMPLEMENTARY STRESS FUNCTION ψ . .	B1
C - PATH INDEPENDENT LINE INTEGRALS FOR STEADY-STATE, TWO-DIMENSIONAL THERMOELASTICITY	C1

List of Figures

<u>Figure</u>	<u>Page</u>
1-1 Schematic of Cracked Plate Subjected to Rapid Thermal Pulses	3
2-1 Influence Function Concept for Calculating Stress Intensity Factor	14
2-2 Concept of superposition for Multiple Point Heat Sources	15
2-3 Concept of Green's Function Integration in Time Domain	16
2-4 Single Edge Cracked Plate Configuration	17
2-5 Center Cracked Plate Configuration	18
2-6 Uncracked Plate for Thermal Stress Solution	19
2-7 Infinite Plate Strip Subjected to Edge Loads	20
3-1 AF-CRACK Software Architecture	30
3-2 Geometry Input Module Menu	31
3-3 Material Input Module Menu	32
3-4 Heat Source Data Input Module Menu	33
3-5 K-Calculation Module Menu	34
3-6 Review Module Menu	35
3-7 Verification Problem Comparison of Steady-State Stress Distribution at $y=0$	36
3-8 Comparison of Stress Intensity Factors for Verification Problem	37
3-9 Finite Element Mesh for the Verification Problem	38
4-1 Sample Problem 1	42
4-2 Stress Distribution at $y=0$ for Sample Problem 1 ($\sigma_{xy}=0$)	43

List of Figures (Concluded)

<u>Figure</u>	<u>Page</u>
4-3 Stress Intensity Factors for Sample Problem 1 . .	44
4-4 Green's Functions for Sample Problem 1 (Mode I only, Mode II = 0)	45
4-5 Sample Problem 2	46
4-6A Stress Distribution for Sample Problem 2 (σ_{yy}) . .	47
4-6B Stress Distributions for Sample Problem 2 (σ_{xy}) .	48
4-7 Stress Intensity Factors for Sample Problem 2 (the same curves for both crack tips)	49
4-8 Green's Functions Due to Q_1 for Sample Problem 2 (Q_2 has similar curves)	50

1.0 INTRODUCTION AND PROBLEM STATEMENT

Analytical techniques are needed by the Air Force for predicting stress intensity factors of cracked metallic structures subjected to rapid thermal pulses. A schematic of such a problem application is illustrated in Figure 1-1. General purpose numerical techniques such as finite element methods are currently available for the solution of such problems. However, they require time-consuming finite element modeling of the structural configuration, including the crack, and detailed thermal/stress analysis must be performed for each thermal transient to be addressed.

The modeling is further complicated by the extremely steep stress gradients which exist in the vicinity of the crack tip. The stress singularities at the crack tip dictate the use of an extremely fine finite element mesh in this region, or a special element which has the appropriate crack tip singularity built into the element interpolation functions. Furthermore, multiple finite element models and analyses are required for a single structure if we desire the stress intensity factors as a function of crack size, which is usually the case.

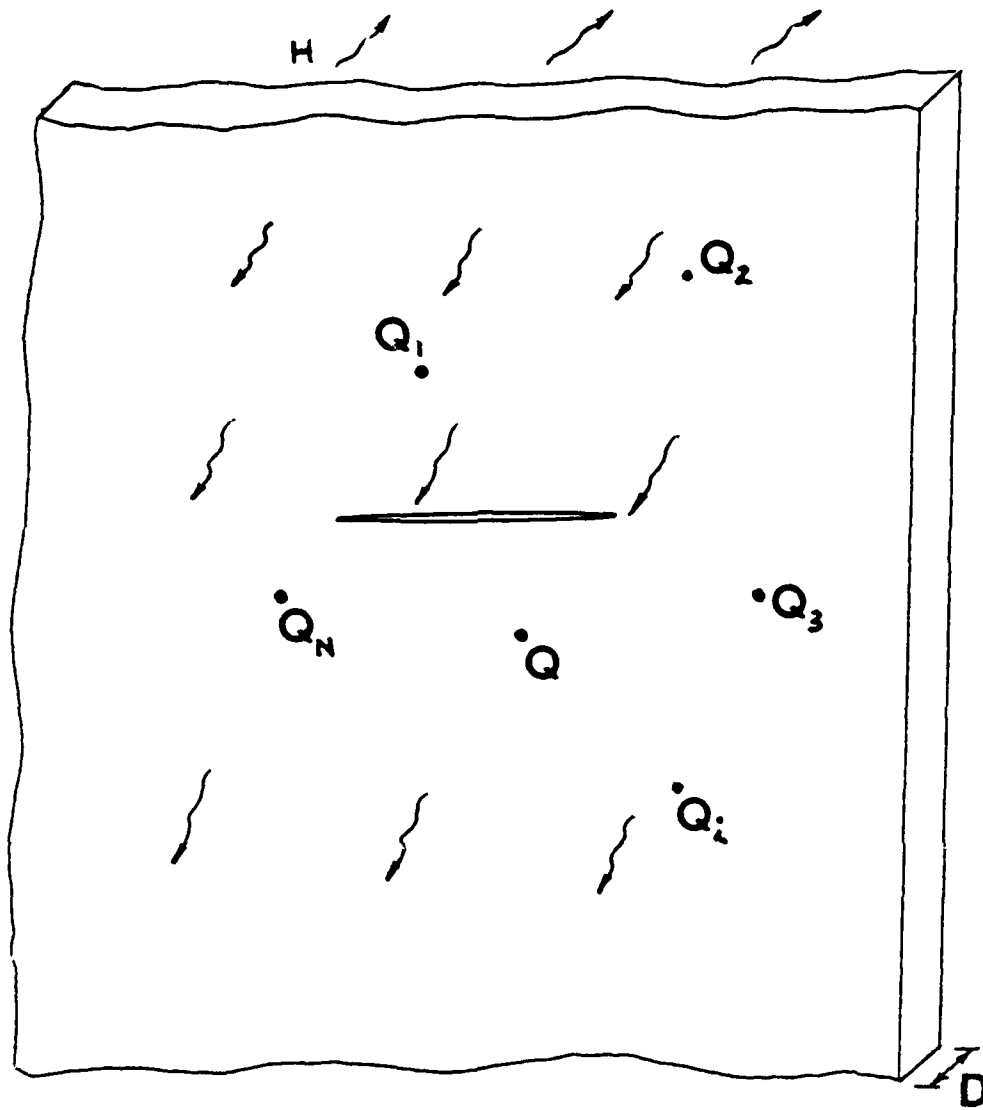
Thus, the objective of this study is to provide a convenient and accurate way to calculate the stress intensity factors caused by rapid thermal pulses, for use in conjunction with existing fracture mechanics software used by the Air Force to predict crack growth and fracture in flaw tolerant design applications.

As a result of the Phase I effort reported here, a preliminary version of an IBM-PC based computer program, AF-CRACK, has been developed based on the concepts of

Green's function and influence function. AF-CRACK calculates stresses and stress intensity factors by integrating the closed-form Green's function solutions to the general thermoelasticity problem of a point heat source in a flat plate containing a crack. For a given plate/crack geometry, the stress distribution and stress intensity factors due to any number of randomly located heat sources (or sinks) can be calculated by AF-CRACK in a few minutes. Preliminary verification of the program shows that results generated by AF-CRACK are very close to those obtained by finite element methods.

AF-CRACK combines and links several independent program modules using a unique "software bus" concept, and is a menu driven, user-friendly software package with extensive graphics capabilities. Both input and graphics in AF-CRACK use the popular spread-sheet program, LOTUS-123 [1], linked directly into the AF-CRACK program through the software bus. In this manner, data input, manipulation and review are greatly facilitated using LOTUS-123's extensive data management and graphics capabilities.

The stress intensity factor results generated by AF-CRACK are useful as input to any of a number of fatigue crack growth and fracture prediction programs used by the Air Force. An example of such a program, Structural Integrity Associates' pc-CRACK computer program has been included on the AF-CRACK software bus. Although a direct data link between the two programs could not be developed under the cost and schedule limitations of the current Phase I effort, stress intensity results generated with AF-CRACK can be directly input to pc-CRACK using the K_I input option in the pc-CRACK LEFM module. If a Phase II effort is funded, a direct link can be developed between AF-CRACK and any companion fracture mechanics software selected by the Air Force.



$\dot{Q}_i = F_i(t)$ - Point Heat Sources at Various Locations in Structure

Figure 1-1. Schematic of Cracked Plate Subjected to Rapid Thermal Pulses

2.0 THEORETICAL SOLUTION

2.1 Assumptions

The following assumptions have to be made to simplify the problem:

(a) The problem is assumed to be plane stress. In other words, the thickness D in Figure 1-1 is assumed to be small enough so that the temperature distribution in the thickness direction can be treated as uniform.

(b) The metallic materials are assumed to be isotropic, homogeneous, and linear elastic.

(c) The rate of heat application is slow enough that the coupling terms and inertia terms in the general thermoelasticity equations can be neglected, i.e. it is assumed that quasi-static thermoelasticity applies. It is anticipated, however, that Green's functions could be found which would permit the incorporation of inertia terms into advanced versions of the software, if it is necessary for envisioned applications.

(d) The crack surfaces are assumed to be stress free and heat conductant. Although the solution techniques developed in this report can also be extended to cracks with insulated surfaces, for purposes of this Phase I feasibility study, the crack surfaces were assumed to be fully heat conductant. In reality, actual crack surfaces are expected to be somewhere between 100 percent heat conductant and insulated.

(e) We assume that the heat convection coefficients remain constant. Again, this assumption was included for purposes

of the Phase I study. Variable heat convection coefficients could be incorporated in the program through a more complicated but similar derivation.

2.2 Governing Stress Solutions

For a plane stress thermoelasticity problem as illustrated in Figure 1-1, the governing equations are

$$\xi \nabla^2 T = T_{,t} + \xi \eta^2 T \quad (1)$$

$$\sigma_{ij,j} = 0 \quad (2)$$

$$\sigma_{ij} = 2G [\epsilon_{ij} + (\frac{\nu}{1-\nu}) \delta_{ij} \epsilon_{kk} - \alpha (\frac{1+\nu}{1-\nu}) \delta_{ij} T] \quad (3)$$

$$\epsilon_{ij} = (U_{i,j} + U_{j,i})/2 \quad (4)$$

and

$$\nabla^2 U_i + (\frac{1+\nu}{1-\nu}) U_{j,ji} = 2 (\frac{1+\nu}{1-\nu}) \alpha T \quad (5)$$

where $T=T(x_1, x_2, t)$ is temperature distribution, t and x_i are time and Cartesian coordinates respectively, $\xi=(K/\rho c)$, K is heat conduction coefficients, ρ is mass density, c is heat capacity, $\eta^2=(2H)/K/D$, H is heat convection from the plate surfaces to the environment (see Figure 1-1), D is the plate thickness, U_i are displacements, α is coefficient of thermal expansion, and G and ν are shear modulus and Poisson's ratio respectively.

Nominal stress distributions generated with these equations are used to develop stress intensity factors via the influence function approach described below.

2.3 Stress Intensity Factor Influence Functions

For any plate/crack geometry, [2] cracktip stress intensity factors can be determined by integrating the product of the stresses at the crack location in the uncracked structure and an influence function (or weight function). That is, for a crack as shown in Figure 2-1, the stress intensity factor can be calculated by

$$K_I = \int_0^a \sigma_{yy}(x) m_1(x) dx \quad (6)$$

$$K_{II} = \int_0^a \sigma_{xy}(x) m_2(x) dx \quad (7)$$

where $m_1(x)$ and $m_2(x)$ are influence functions and σ_{ij} are the normal and shear stress distributions on the cracked surface in an indentical but uncracked plate which is under the same temperature distribution as the cracked plate.

Appendix A includes influence functions for a single edge cracked plate and a center cracked plate, presented by Bueckner [2] and Tada [3] respectively. Many such influence functions for other crack models of interest are available in the literature, and can be added as the need arises.

2.4 Principle of Superposition

In general, as shown in Figure 2-2, there may be multiple heat sources (or sinks) within the plate which will cause

thermal stresses and stress intensity factors at cracks in the structure. Since the problem is linear, it is easily demonstrated that total stress intensity factor can be calculated as the sum of the stress intensity factors caused by each individual heat source, acting independently. That is

$$K(t) = \sum_i [K(t)]_i \quad (8)$$

where $K(t)$ is the total stress intensity factor and $[K(t)]_i$ is the stress intensity factor due to the i^{th} heat source.

2.5 Green's Function for Time Integration

In equation (8), the stress intensity factor $[K(t)]_i$ caused by each individual heat source can be solved with the concept of Green's function integration. As illustrated in Figure 2-3, the stress intensity factor due to a heat source $Q(t)$ can be calculated by

$$[K(t)]_i = \int_0^t Q_i(\tau) G(t-\tau) d\tau \quad (9)$$

where $G(t)$ is the stress intensity factors due to a Delta function $\delta(t)$ heat source at the i^{th} heat source location.

As shown in Figure 2-3, generally, the Green's function $G(t)$ will decay and approach to zero after a decay period t_d . Therefore, the integration range in equation (9) can be reduced to from $(t-t_d)$ to t . Such a reduction in the integration range greatly increases the speed of the

calculation because, instead of integrating for the entire time history, it is only necessary to integrate backwards from the present time t to $(t-t_d)$ as follows

$$[K(t)]_i = \int_{t-t_d}^t Q_i(\tau) G(t-\tau) d\tau \quad (9a)$$

2.6 Single Edge Cracked Plate and Center Cracked Plate

For Phase I, only two crack models, single edge cracked plates (Figure 2-4) and center cracked plates (Figure 2-5) are considered. We also assumed that, similar to the heat convection coefficient H on the plate surfaces, the heat convection coefficients H_1 and H_2 at the edges of the plate remain constant.

Previous sections show that the stress intensity factors for both crack models can be easily obtained by equations (6 through 9) if the stress distribution, resulting from a delta function heat source (or sink) $Q\delta(t)$ at any arbitrary location (x',y') in the uncracked plate (Figure 2-6), can be solved.

To solve for the Green's function, the following boundary conditions need to be included:

at $x = 0$,

$$KT_{,x} = -H_1 T \quad (10)$$

$$\sigma_{xx} = \sigma_{xy} = 0 \quad (11)$$

at $x=B$,

$$KT_{,x} = H_2 T \quad (12)$$

$$\sigma_{xx} = \sigma_{xy} = 0 \quad (13)$$

at $y = \pm\infty$,

$$T = 0 \quad (14)$$

$$\sigma_{xx} = \sigma_{yy} = \sigma_{xy} = 0 \quad (15)$$

The temperature solution to the uncracked plate problem, shown in Figure 2-6, can be obtained in closed form by the standard method of separation of variables [4]. The result is

$$T(x,y,t) = \frac{Q}{2\rho c \delta \sqrt{\pi \xi t}} \sum_n (Z_n(x) Z_n(x')) \exp[-\xi \alpha_n^2 t - \xi \eta^2 t - \frac{(y-y')^2}{4\xi t}] \quad (16)$$

where

$$\tan \alpha_n B = \frac{\alpha_n K(H_1 + H_2)}{K^2 \alpha_n^2 - H_1 H_2} \quad (17)$$

$$Z_n(x) = (K \alpha_n \cos \alpha_n x + H_1 \sin \alpha_n x) Y_n \quad (18)$$

$$Y_n^2 = \frac{2(K^2 \alpha_n^2 + H_2^2)}{(K^2 \alpha_n^2 + H_1^2) [B(K^2 \alpha_n^2 + H_2^2) + K H_2] + K H_1 (K^2 \alpha_n^2 + H_2^2)} \quad (19)$$

The next step is to solve for the stress distribution due to the temperature field equation (16). References [5,6] show that one particular solution to the thermal stress problem can be expressed in terms of a stress function ϕ as follows

$$U_i = \phi_{,i} \quad (20)$$

$$\sigma_{xx} = -2G \phi_{,yy} \quad (21)$$

$$\sigma_{yy} = -2G \phi_{,xx} \quad (22)$$

$$\sigma_{xy} = 2G \phi_{,xy} \quad (23)$$

$$\phi(x,y,t) = \alpha(1+\nu) e^{-\xi\eta^2 t} \int_0^t e^{\xi\eta^2 \tau} T(x,y,\tau) d\tau + \phi_0 \quad (24)$$

where ϕ is a stress function, and ϕ_0 is a function of x , y , and t such that ϕ would remain finite as t approaches infinity. Substitution of equation (16) into equation (24) yields

$$\phi = e^{-\xi\eta^2 t} \sum \phi_n \quad (25)$$

where

$$\begin{aligned} \phi_n = \frac{-\alpha(1+\nu)Q}{4\rho c D \alpha_n} z_n(x) z_n(x') [e^{-\alpha_n(Y-Y')} \operatorname{erfc}(\omega_1) + \\ e^{\alpha_n(Y-Y')} \operatorname{erfc}(\omega_2)] \end{aligned} \quad (26)$$

$$\omega_{1,2} = (\alpha_n^2 \xi t)^{1/2} \pm \frac{(y-y')}{\sqrt{4\xi t}} \quad (27)$$

and $\text{erfc}(x)$ is a complementary error function.

In general, the particular solution ϕ shown in equations (25 through 27) does not satisfy the stress free boundary, equations (11 and 13), at $x=0$ and $x=B$. A complementary solution ψ , which is an analytic function, must be included to make the two edges $x=0$ and $x=B$ stress free. The stresses are then calculated by

$$\sigma_{xx} = 2G (\psi - \phi)_{,yy} \quad (28)$$

$$\sigma_{yy} = 2G (\psi - \phi)_{,xx} \quad (29)$$

and

$$\sigma_{xy} = -2G (\psi - \phi)_{,xy} \quad (30)$$

where ψ is the solution of

$$\nabla^2 \nabla^2 \psi = 0 \quad (32)$$

$$\psi_{,yy} = \phi_{,yy} \quad \text{at } x=0 \text{ and } x=B \quad (33)$$

and

$$\psi_{,xy} = \phi_{,xy} \quad \text{at } x=0 \text{ and } x=B \quad (34)$$

Solution to equations (32 through 34) can be obtained by the methods described in [7] for the problem of an infinite strip of plate subjected to arbitrary tractions at both edges (as illustrated in Figure 2-7), and is summarized in Appendix B.

Therefore, at the cross section of $y=0$, the stresses caused by a Delta function heat source $Q\delta(t)$ at (x',y') are

$$\sigma_{yy} = \hat{\sigma}_{yy} + \sum (P_n \cos \alpha_n x + Q_n \sin \alpha_n x) \quad (35)$$

$$\sigma_{xy} = \hat{\sigma}_{xy} + \sum (R_n \cos \alpha_n x + S_n \sin \alpha_n x) \quad (36)$$

where $\hat{\sigma}_{yy}$ and $\hat{\sigma}_{xy}$ are stresses due to the complementary stress function ψ and are listed in Appendix B,

$$P_n = \frac{G\alpha(1+\nu)Q}{2\rho cD} Y_n K \alpha_n^2 M Z_n(x') \quad (37)$$

$$Q_n = \frac{G\alpha(1+\nu)Q}{2\rho cD} Y_n H_1 \alpha_n M Z_n(x') \quad (38)$$

$$R_n = \frac{G\alpha(1+\nu)Q}{2\rho cD} Y_n H_1 N Z_n(x') \quad (39)$$

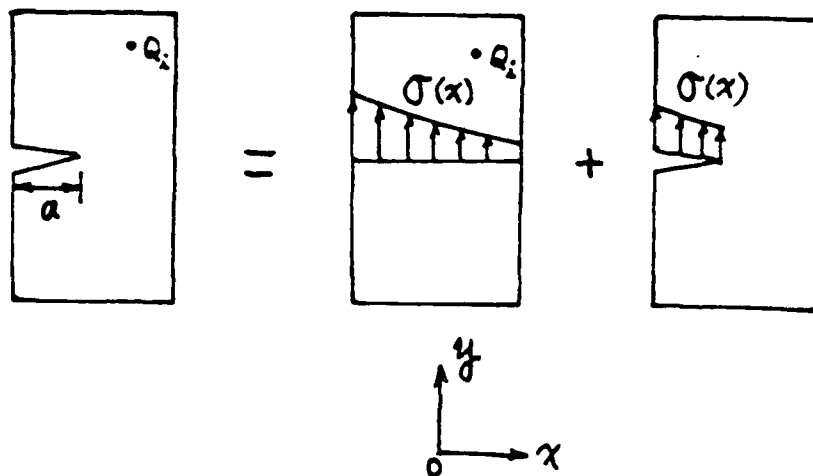
$$S_n = - \frac{G\alpha(1+\nu)Q}{2\rho cD} Y_n K \alpha_n N Z_n(x') \quad (40)$$

$$M = - [\exp(\alpha_n y') \operatorname{erfc}(\omega_2) + \exp(-\alpha_n y') \operatorname{erfc}(\omega_1)] \quad (41)$$

$$N = - \left\{ \exp(\alpha_n y') \left[\alpha_n \operatorname{erfc}(\omega_2) + \frac{\exp(-\omega_2^2)}{\sqrt{\pi \xi t}} \right] - \exp(-\alpha_n y') \left[\alpha_n \operatorname{erfc}(\omega_1) + \frac{\exp(-\omega_1^2)}{\sqrt{\pi \xi t}} \right] \right\} \quad (42)$$

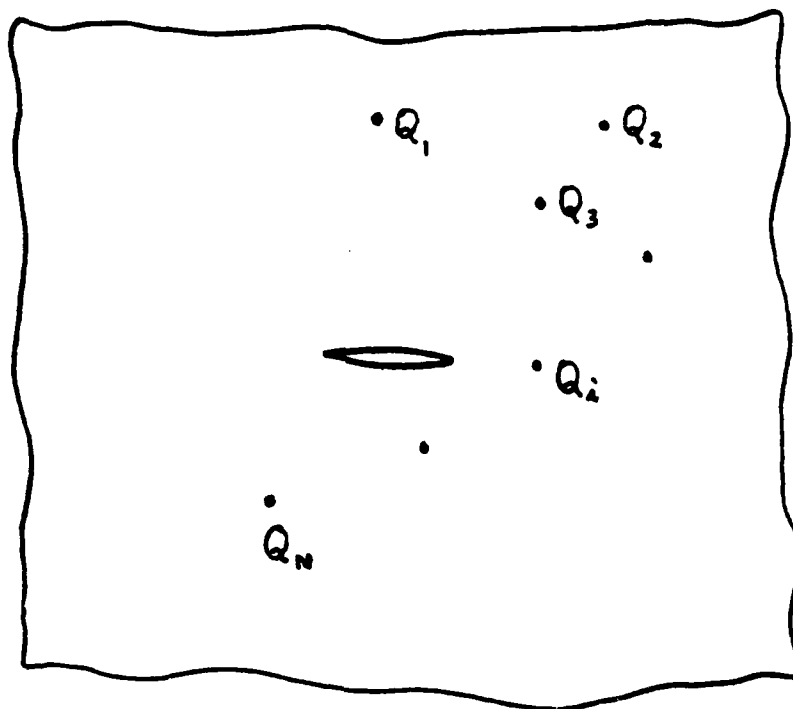
The Green's functions for the stress intensity factors can, thereby, be calculated by substituting equations (35 and 36) into equations (6 and 7), and the total stress intensity factors can be obtained by summing up equation (9) for all heat sources or sinks in the plate.

Verification of the above methodology is provided in Section 3.3, and its application to two sample problems is illustrated in Section 4.0.



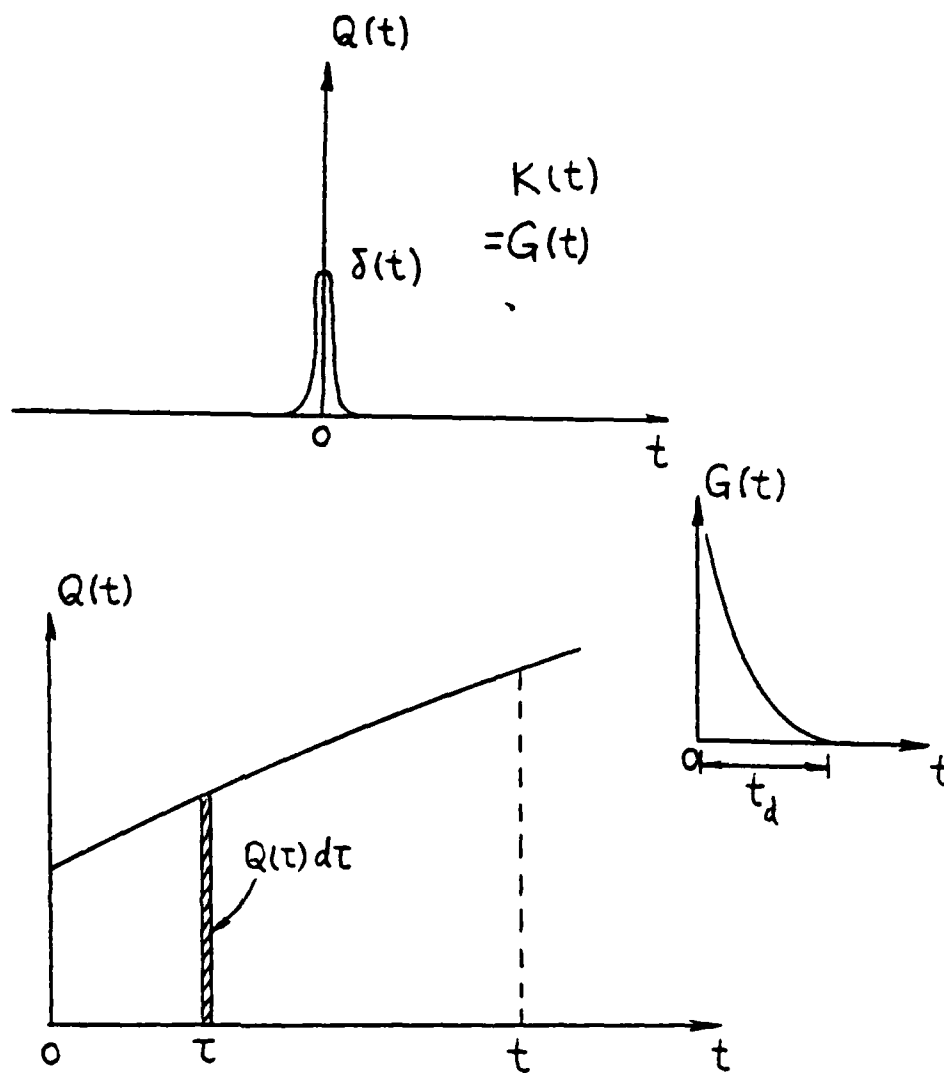
$$K(t) = \int_0^a \sigma(x, t) \cdot m(x) dx$$

Figure 2-1. Influence Function Concept for Calculating Stress Intensity Factor



$$K(t) = \sum_{i=1}^N [K(t)]_i$$

Figure 2-2. Concept of Superposition for Multiple Point Heat Sources



$$K(t) = \int_0^t Q(\tau) G(t-\tau) d\tau$$

$$= \int_{t-t_d}^t Q(\tau) G(t-\tau) d\tau$$

Figure 2-3. Concept of Green's Function Integration in Time Domain

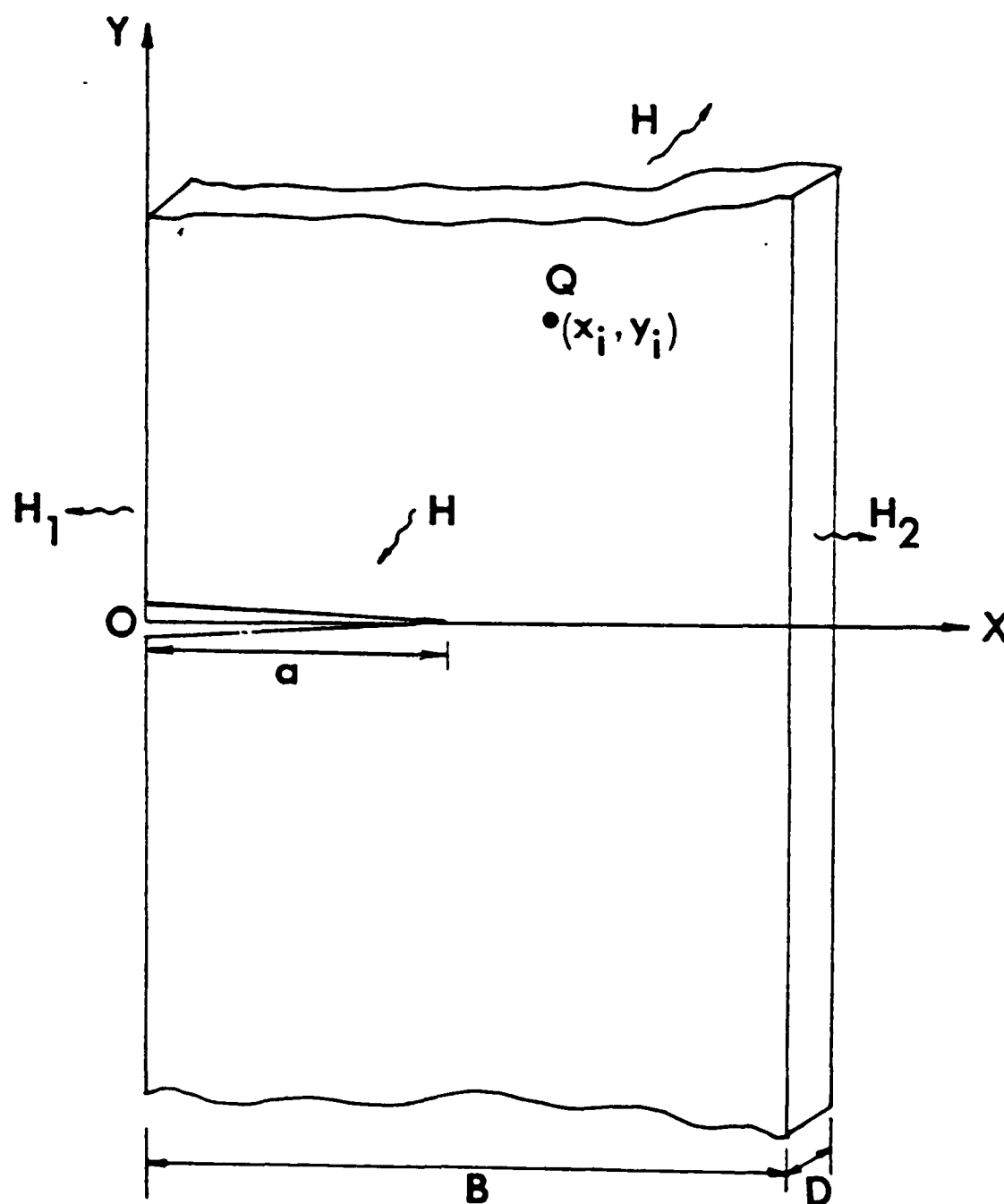


Figure 2-4. Single Edge Cracked Plate Configuration

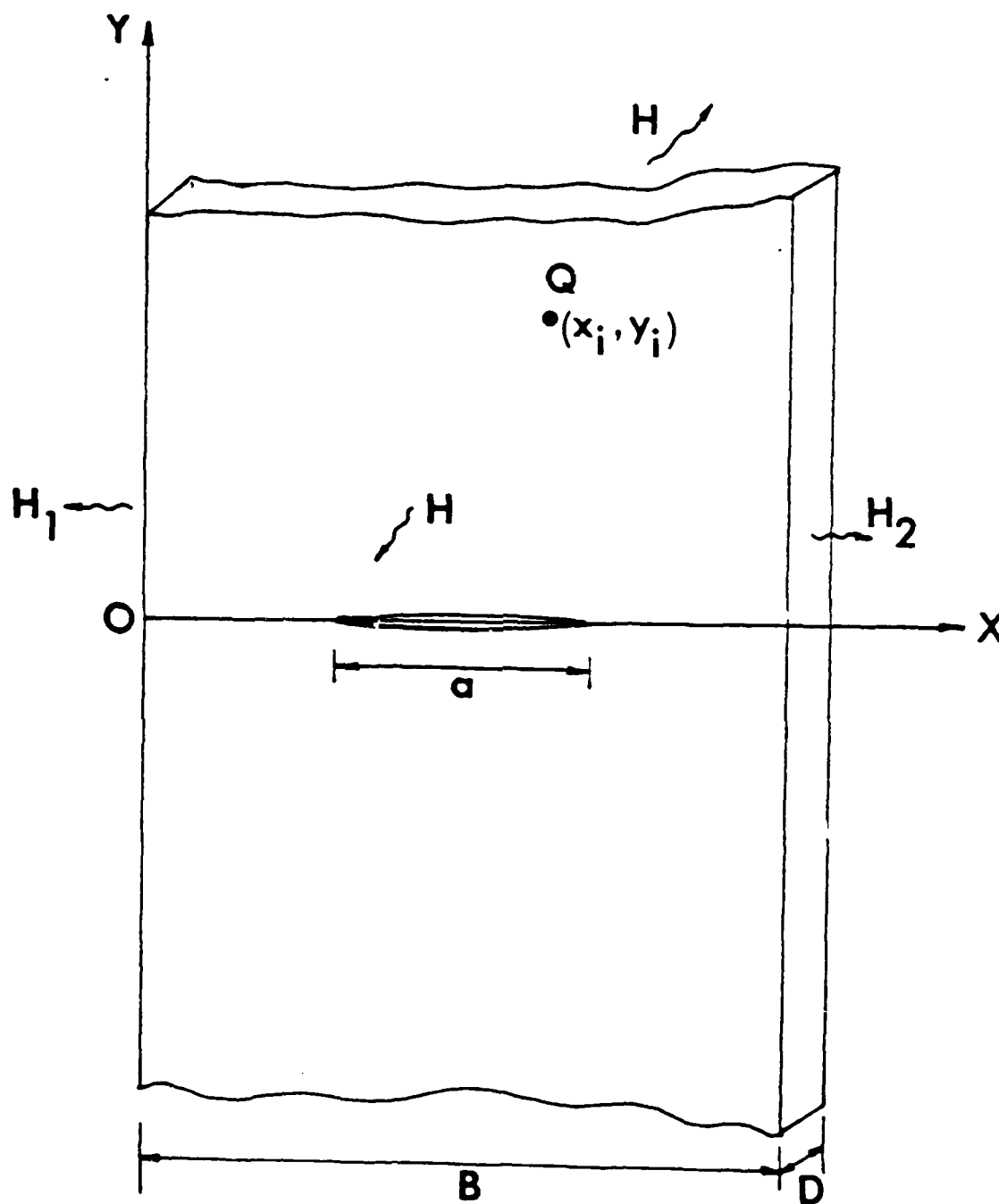


Figure 2-5. Center Cracked Plate Configuration

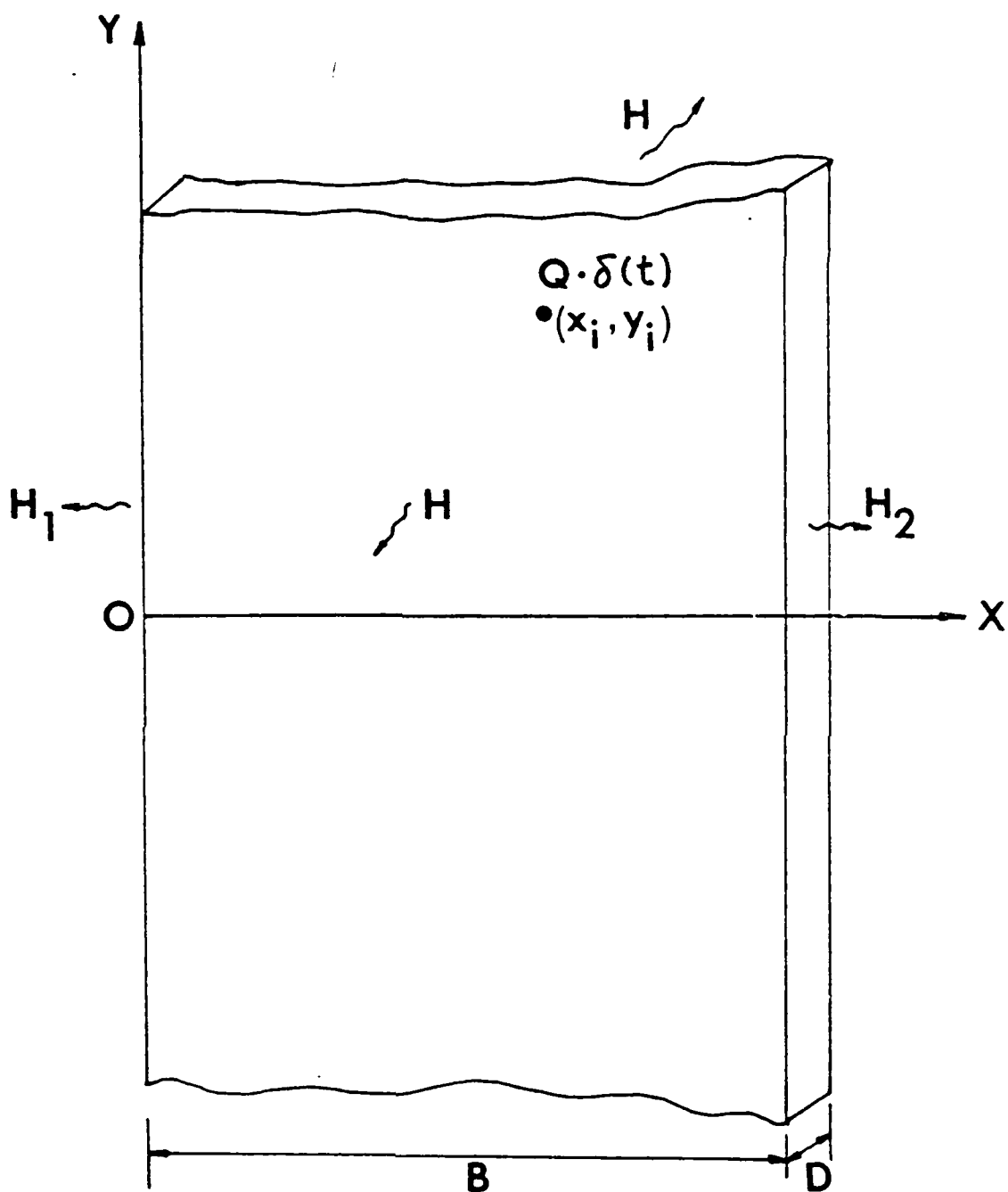


Figure 2-6. Uncracked Plate for Thermal Stress Solution

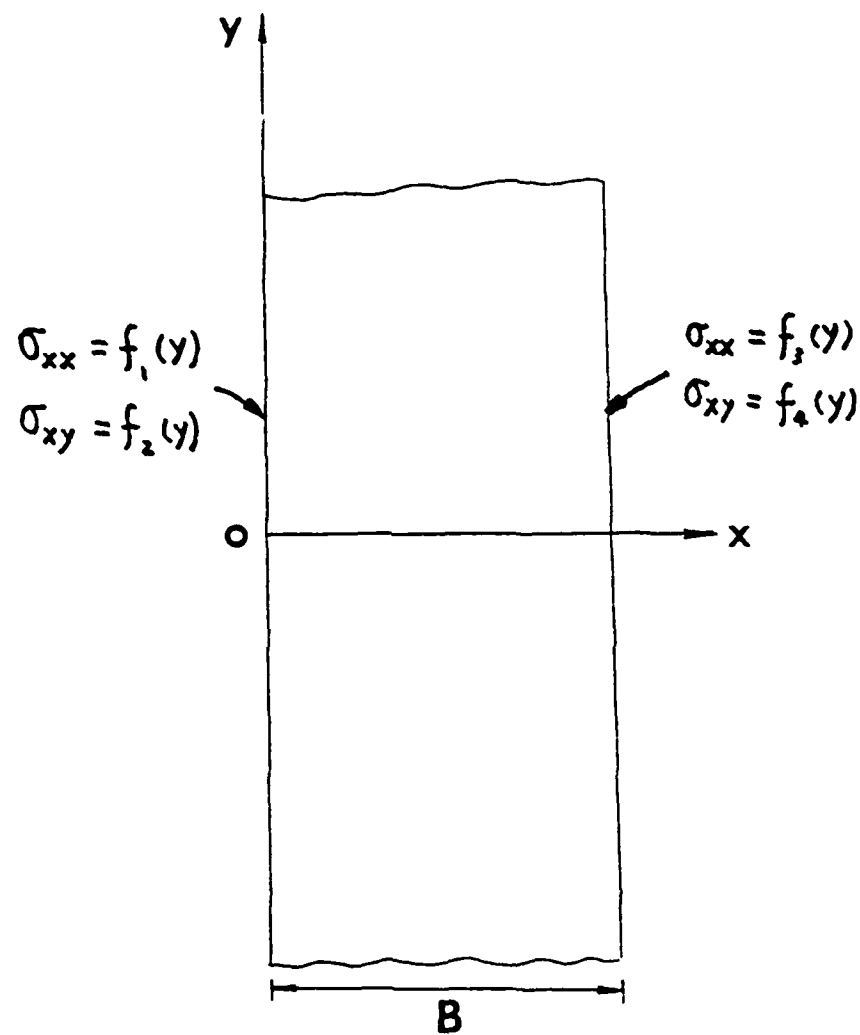


Figure 2-7. Infinite Plate Strip Subjected to Edge Loads

3.0 PHASE I DEMONSTRATION SOFTWARE (AF-CRACK)

3.1 General Program Features

The theoretical solution technique described in Section 2.0 has been implemented in the form of a demonstration software package called AF-CRACK. Although preliminary in nature, this software package incorporates an interactive, menu-driven format, which permits its use without extensive skills on the computer or operating system, and without constant reference to a user's manual. Also, because it is modularized, a user can stop at any point during a problem application and come back later to finish the calculation at any time.

The program runs on an IBM PC-XT or -AT (or compatible) with minimum of 640K memory. A math co-processor card is also recommended (although not mandatory) to enhance program execution speed. All of the AF-CRACK input and output are unit-transparent. The user can use any set of units he or she wishes as long as all the data are consistently in the same unit system. The following sections describe the structure and execution of the AF-CRACK program, as well as verification problems run to compare the results to other solution techniques.

3.2 Software Architecture

The basic structure of the AF-CRACK computer program is illustrated in Figure 3-1. The program consists of six independent modules and one data base shared by all the modules. A "software bus" concept, developed independently by Structural Integrity Associates [8], was used to link the program modules and the data base. The software bus allows

users to enter, execute and exit each program module with a single key stroke, as well as to execute other, independent software, which can be set up to interface with the same data base. (Some customization of data files is required, however, in order for AF-CRACK to automatically transfer data with other independent software packages on the bus.)

As illustrated in Figure 3-1, AF-CRACK currently contains six modules: Geometry Input, Material Input, Heat Source Data Input, K Calculation, pc-CRACK, and Review. The last two modules, pc-CRACK and Review actually incorporate two pre-existing software packages which are useful in pre- or post-processing the AF-CRACK results. The Review module loads up the popular LOTUS-123 spreadsheet and graphics software, which is used to generate tabular input to some program modules, and to create tables and graphical displays of the results. Translation routines are included which automatically link AF-CRACK input and output files with LOTUS-123.

PC-CRACK refers to another menu-driven fracture mechanics program developed independently by Structural Integrity Associates [9], which possesses a wide variety of crack growth, critical flaw size and elastic plastic fracture mechanics capabilities. The long term objective is to be able to directly feed the stress intensity factor results from AF-CRACK into PC-CRACK (or some other similar program of Air Force's choice) for further analyses, such as fatigue crack propagation, critical crack size, and corrosion crack growth. However, at the present stage, the data base generated by AF-CRACK is not compatible with the input format of PC-CRACK. Full communication between AF-CRACK and PC-CRACK can be achieved later if Phase II of this project is pursued.

Copies of these two independent software packages, along with user's manuals are included with this report, as part of the Phase I deliverable. A detailed description of the other AF-CRACK program modules and the data base is given in the following sections.

3.2.1 Geometry Input Module

As shown in the menu for this module illustrated in Figure 3-2, this module has two steps: select crack model and input plate dimensions. In the first step, users are asked to choose between a single edge cracked plate and a center cracked plate. More crack models, such as crack emanating from a hole, semi-elliptical surface crack in a half space, and quater-circular surface crack in a quarter space, can be included in Phase II of this project. Once the crack model is chosen, the user can execute the second step of inputting geometric dimensional data. For the two crack models currently implemented, only plate width B and thickness D are needed. The format for input of the data is self-explanatory.

3.2.2 Material Input

As illustrated in Figure 3-3, this module consists of three major steps: input heat convection constants, H , H_1 , and H_2 , input heat conduction constants, K , ρ , and c , and input elastic constants, E , ν , and α . Once again, the input format is self explanatory.

3.2.3 Heat Source Data

As shown in the menu in Figure 3-4, there are three steps in this module. The first step asks the user to input number of heat sources (or sinks), number of eigen values to be

included, time increment Δt to be used in the computer simulation, and total time for the analysis. The maximum number of eigen values that can be used is currently set to 20. A higher number of eigen value terms will result in longer computer execution in the Green's function calculation. It is recommended that users perform a simple convergence study to get an optimal number of eigen values. The program will choose an optimal Δt for numerical computation based on the material constants and geometrical dimensions of the problem. The optimal time increment Δt is set at $1/30$ of the decay period t_d for the problem. In this preliminary version of AF-CRACK, the total time has to be less than $250(\Delta t)$.

The next step in this module is to input heat source locations (x',y') as well as the starting and ending time for each heat source or sink. When the second step is chosen in this module, the user only needs to input numbers in appropriate cells in the LOTUS-123 spread sheet, which is loaded automatically. Upon leaving this spread sheet, the input data are saved in a text file for later use.

The third step in this module is to input heat source intensity versus time for each heat source. Again, a LOTUS-123 spread sheet will appear on screen and the user only needs to input numbers in the cells. Note that, in this spread sheet, the time t which appears in the first column is the time relative to the starting time specified in the last step. In other words, if a heat source $Q(t)$ does not start to generate heat until t_0 , the user can input the starting time as t_0 in the last step and input $Q(t-t_0)$ in this step. In this spread sheet, the time increment has been set automatically to be the optimal Δt calculated in the first step and the user should not attempt to change it. In the current demonstration version of AF-CRACK, only a

total of 250 steps is allowed for each heat source. Finally, we must mention that the heat source intensity should be positive for heat sources and negative for heat sinks.

3.2.4 Calculate K

Stress distribution and stress intensity due to specified heat sources are calculated in this module. As illustrated in Figure 3-5, there are four steps in this module.

The first step is to input crack length for the selected crack model. The second step is to calculate Green's functions for all the heat sources. The third is to modify heat source intensity versus time sources if the user desires. (This step can be skipped if the user has already defined heat source intensity versus time curves and does not want to modify them.) The last step is to calculate stress intensity factors for the selected crack model under the specified heat sources. Two sets of stress intensity factors are calculated for center cracked plates, one set for each crack tip. Only one set of stress intensity factors is needed for single edge cracked plates.

3.2.5 Data Base

The input and output of all the above modules are saved in several data files. There are two types of data files used in the program: text files and binary files. The text files are tagged with ".PRN" as their extension and the binary files are tagged with ".DAT" as their extension. For example, "GEOM.PRN" is a text file saved after the geometry input module is executed and "HEAT.DAT" is a binary file saved after the heat source data input module is executed.

3.2.6 Review

This module is used to display the input and output data, either in tabular or graphics format, on the screen. Hard copies of the displays can also be obtained. The commercially available LOTUS-123 spreadsheet/graphics software package is used throughout this module, adding a wide range of input/output options to AF-CRACK. LOTUS-123 compatible files are automatically generated of all key AF-CRACK data, which can then be plotted, printed, or otherwise manipulated, using LOTUS-123's broad range of capabilities.

To facilitate program use by those who are unfamiliar with LOTUS-123, extensive use of "Macro" commands has been included in all the spread sheets. Thus the user simply presses one or two keys as instructed on screen to see a specific plot of his or her results. This review module (Figure 3-6) puts all the data in five different spread sheets, which are called from the Review module menu. The first option obtains a spreadsheet of stress intensity versus time results; the second spread sheet contains Green's functions for each heat source. The third spreadsheet is used to plot stress distribution in the uncracked plate at the cross section of crack, and the fourth is used to show heat source intensity versus time curves. The last spreadsheet provides a display of general problem information, such as crack model, crack length, material constants, etc., in the analysis.

3.3 Program Verification

A preliminary verification has been performed for AF-CRACK by comparing the AF-CRACK results with finite element and pc-CRACK [9] solutions.

The verification problem analyzed is a single edge cracked plate, as shown in Figure 2-4, with the following input:

$$B = 10 \text{ inches}, D = 1 \text{ inch}, a = 2 \text{ inches}$$

$$H = H_1 = H_2 = 0$$

$$K = 0.0002579 \text{ Btu}/(\text{sec-F-in})$$

$$\rho = 0.09734 \text{ lb/in}^3, \quad c = 2.178 \text{ Btu}/(\text{lb-F})$$

$$E = 10 \times 10^6 \text{ psi}, \quad \nu = 0.3, \quad \alpha = 12.73 \times 10^{-6} \text{ in/in/F}$$

$$Q(t) = H(t) \text{ Btu} \quad \text{at} \quad x' = 5 \text{ inches}, \quad y' = 0 \text{ inch},$$

Eigen values included = 20

where $H(t)$ is a Heaviside step function. This verification problem represents a 10 inch wide thin aluminum plate with a 2-inch long edge crack, under a unit step heat source applied at the center of the plate, right in front of the crack tip.

Stress and stress intensity factor K_I for the verification problem, calculated by AF-CRACK, are depicted in Figures 3-7 and 3-8 respectively.

For the same problem, a finite element program, FEM2D [10] was used to predict the steady state temperature as well as thermal stress distributions for the uncracked plate. The finite element mesh used is shown in Figure 3-9, and the resulting stress distributions are also plotted in Figure 3-7 along with the AF-CRACK results. Due to the symmetry conditions at $y=0$, only half of the plate was modeled in

Figure 3-9. A total of 88 eight-node isoparametric elements and 303 nodal points were used in the finite element model. Figure 3-7 shows that the stresses predicted by AF-CRACK are very close to that calculated by finite element. The stress distribution obtained from the finite element analysis was then input into pc-CRACK [9] to calculate the stress intensity factors. The steady-state stress intensity factor predicted by pc-CRACK is shown in Figure 3-8 in conjunction with the AF-CRACK solutions. Again, very good agreement between the two solutions is observed.

Another steady-state stress intensity factor solution has also been obtained by actually modeling the crack in the finite element analysis and calculating the energy release rate by a path-independent line integral, J_1' . Details of J_1' and its related path-independent line integrals are discussed in Appendix C of this report. The finite element mesh used in the J_1' calculation is the same as that illustrated in Figure 3-9 except that part of the symmetry line in the model was set to stress free to reflect the existence of the crack. The energy release rate $J = J_1'$ is then used to calculate the stress intensity factor with the relation between J and K :

$$K_I = \sqrt{J E}$$

where E is the Young's modulus of the material. Stress intensity factor predicted by the line integral J_1' is also plotted in Figure 3-8 which illustrates that the steady-state stress intensity factors predicted by AF-CRACK and the other two independent methods are within 1% of each other.

More verification problems are needed to fully test the program in the next phase of the project. Numerically, it is necessary to run more finite element analyses, both steady state and transient, for more crack geometries and sizes. It would also be desirable to verify the program experimentally, by conducting some tests to measure the stress and stress intensity factors in plates or other structures under rapid thermal pulses. Verification by testing will also be proposed as part of the Phase II effort.

Nonetheless, based on the preliminary verification performed here, we conclude that the AF-CRACK methodology is capable of predicting stress intensity factors for structures under rapid thermal pulses, accurately, and with only a small fraction of the computer time and manpower required by the conventional finite element analyses. Full development of the AF-CRACK program will thus greatly enhance the capability of the Air Force for predicting stress intensity factors and performing subsequent fracture mechanics analyses.

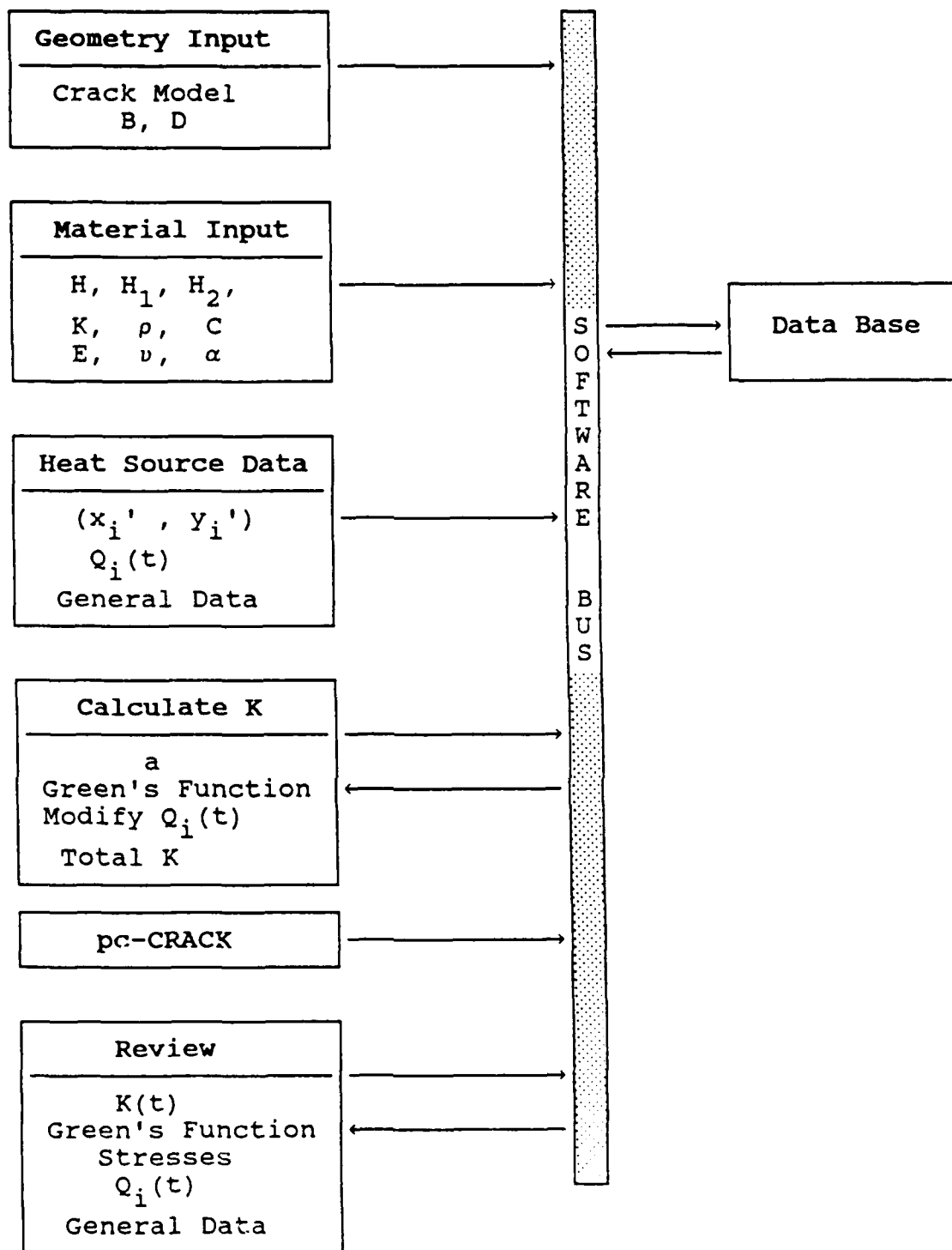


Figure 3-1. AF-CRACK Software Architecture

INPUT GEOMETRIC DATA (GEOM)
MODULE MENU

USER OPTIONS:

- + 1- CHOOSE CRACK MODEL
- 2- INPUT GEOMETRIC DIMENSIONS
- 3- TERMINATION

Cursor Controls

- + Current Line
- ↑ Moves Up
- ↓ Moves Down
- ← Selects Option
- Fx Selects Option x

- x)10 Use Shift
- + Function Key
- (F11= Shift+F1)

Figure 3-2. Geometry Input Module Menu

INPUT MATERIAL CONSTANTS (MATL)
MODULE MENU

USER OPTIONS:

- + 1- INPUT HEAT CONVECTION COEFFICIENTS
- 2- INPUT HEAT TRANSFER CONSTANTS K, RHO, C
- 3- INPUT ELASTIC CONSTANTS, E, NU, ALPHA
- 4- TERMINATION

Cursor Controls

- + Current Line
- ↑ Moves Up
- ↓ Moves Down
- ← Selects Option
- Fx Selects Option x

- x>10 Use Shift
- + Function Key
- (F11= Shift+F1)

Figure 3-3. Material Input Module Menu

INPUT HEAT SOURCE DATA (HEAT)
MODULE MENU

USER OPTIONS:

- + 1- INPUT GENERAL INFORMATION
- 2- INPUT SOURCE LOCATION AND ON-OFF TIME
- 3- INPUT HEAT SOURCE INTENSITY VS TIME
- 4- TERMINATION

Cursor Controls

- + Current Line
- ↑ Moves Up
- ↓ Moves Down
- ← Selects Option
- Fx Selects Option x

- x>10 Use Shift
- + Function Key
- (F11= Shift+F1)

Figure 3-4. Heat Source Data Input Module Menu

CALCULATE K BY GREEN'S FUNCTION (GREN)
MODULE MENU

USER OPTIONS:

- + 1- INPUT CRACK LENGTH
- 2- CALCULATE GREEN'S FUNCTIONS
- 3- INPUT OR MODIFY Q VS TIME CURVES
- 4- CALCULATE K
- 5- TERMINATE

Cursor Controls

- + Current Line
- ↑ Moves Up
- ↓ Moves Down
- ← Selects Option
- Fx Selects Option x

- x>10 Use Shift
- + Function Key
- (F11= Shift+F1)

Figure 3-5. K-Calculation Module Menu

REVIEW RESULTS (REVM)
MODULE MENU

USER OPTIONS:

- + 1- PLOT K VERSUS TIME
- 2- PLOT GREEN'S FUNCTIONS
- 3- PLOT STRESS DISTRIBUTION AT $y=0$
- 4- PLOT Q VERSUS TIME
- 5- REVIEW INPUT DATA
- 6- TERMINATION

Cursor Controls

- + Current Line
- ↑ Moves Up
- ↓ Moves Down
- ← Selects Option
- Fx Selects Option x

- x>10 Use Shift
- + Function Key
- (F11= Shift+F1)

Figure 3-6. Review Module Menu

COMPARISON OF STRESS RESULTS

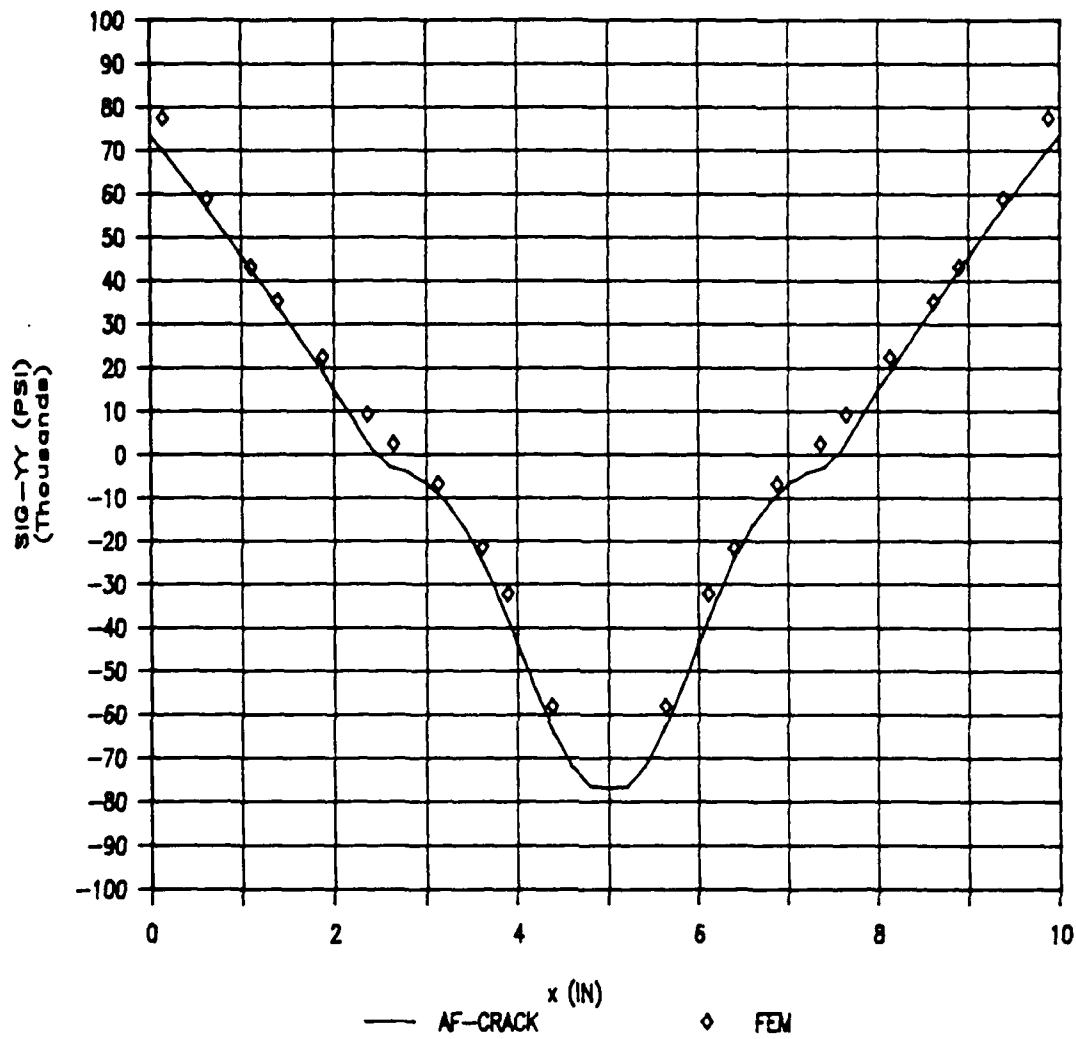


Figure 3-7. Verification Problem Comparison of Steady-State Stress Distribution at $y = 0$

STRESS INTENSITY FACTORS

VERIFICATION PROBLEM

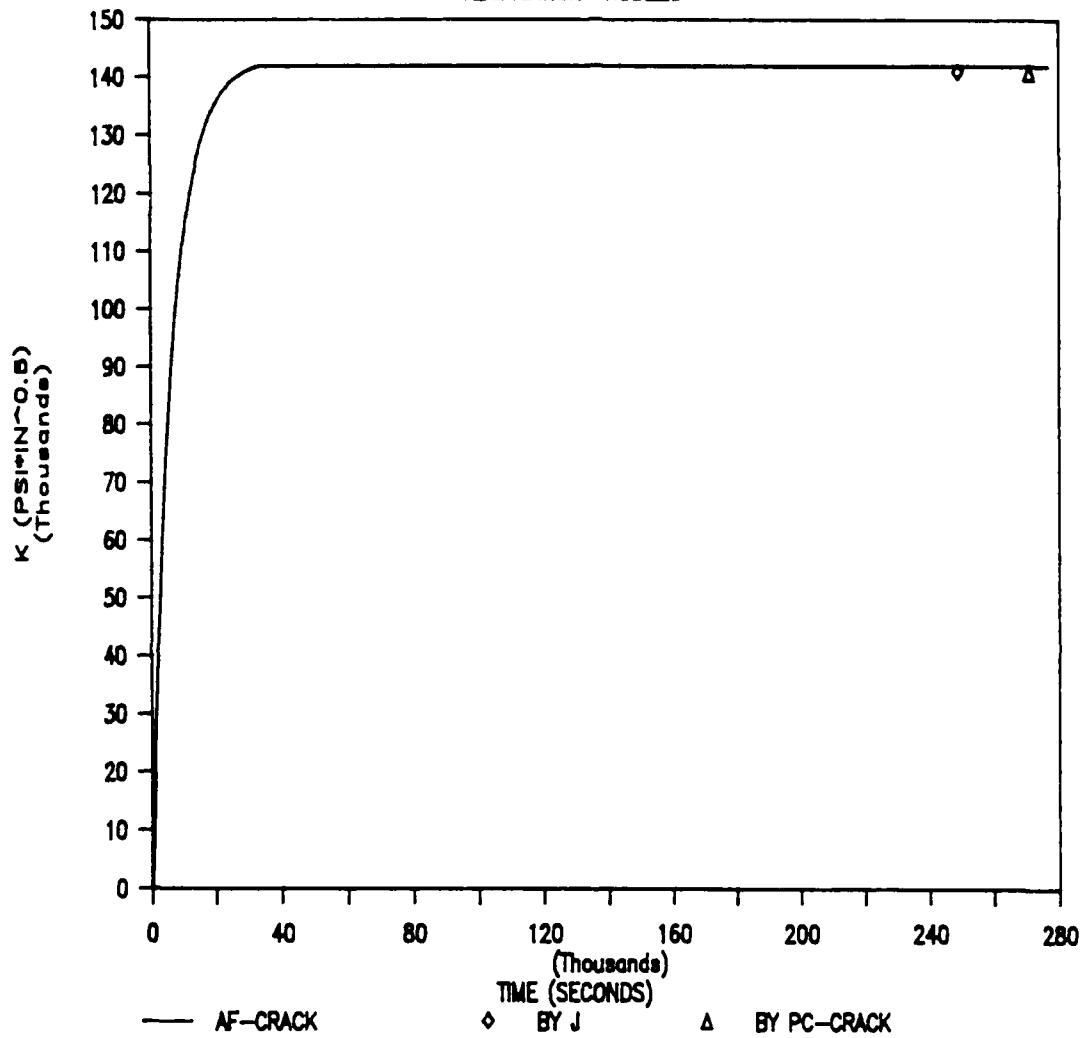


Figure 3-8. Comparison of Stress Intensity Factors for Verification Problem

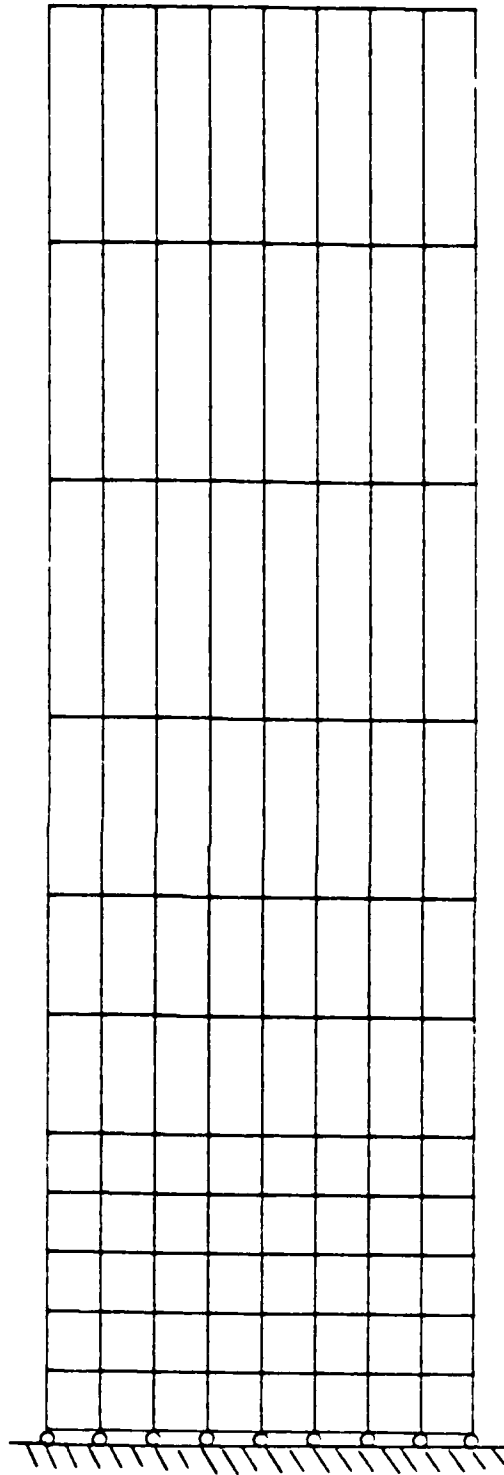


Figure 3-9. Finite Element Mesh for Verification Problem

4.0 SAMPLE PROBLEMS

Two sample problems are presented in this section to illustrate the use of the AF-CRACK program. Except for crack model, crack size, heat transfer coefficient and heat source specification, all other parameters for the two sample problems are the same, and are as follows:

$$B = 10 \text{ inches}, D = 0.2 \text{ inch}$$

$$K = 0.0002579 \text{ Btu}/(\text{sec-F-in})$$

$$\rho = 0.09734 \text{ lb/in}^3, \quad c = 2.178 \text{ Btu}/(\text{lb-F})$$

$$E = 10 \times 10^6 \text{ psi}, \quad \nu = 0.3, \quad \alpha = 12.73 \times 10^{-6} \text{ in/in/F}$$

$$\text{Eigen values included} = 50$$

The above material properties are representative of aluminium.

4.1 Sample Problem 1 - Single Edge Cracked Plate

As shown in Figure 4-1, this sample problem considers a continuous surface crack, 2 inches deep, at the left edge of the above plate. The heat convection coefficients used in this problem are

$$H = H_1 = H_2 = 0.0001929 \text{ Btu}/(\text{sec-F-in}^2)$$

and the four heat sources are at (x,y) coordinates of (10,4), (10,2), (10,-2), and (10,-4) with

$$Q_1 = Q_2 = Q_3 = Q_4 = H(t-150) - H(t-1200) \quad \text{Btu}$$

where $H(t)$ is a Heaviside step function. As can be seen in Figure 4-1, this simulates a line heat loading at the right edge of the plate, which steps on at 150 seconds, and off again at 1200 seconds.

Resulting stress distributions for the uncracked plate are illustrated in Figure 4-2, at various times during the loading. The stress pattern consists of compression near the heat sources, and tension near the edge crack. This shape remains constant as the stress builds up to its maximum value, following application of the load, and then subsides as the load is removed. The resulting stress intensity factors versus time are illustrated in Figure 4-3. From this figure, we can see that the mode I stress intensity factor, K_I , begins to rise at the time of load application (150 seconds), levels out at a maximum value at about 600 seconds, and then decays to zero again after the load is removed at 1200 seconds. As expected due to problem symmetry, the mode II stress intensity factor is shown as zero throughout the problem; however, this was not calculated by the program since the single edge crack plate model does not yet incorporate the mode II influence functions. Green's functions showing the stress intensity factor response to a unit spike loading at each of the heat sources are illustrated in Figure 4-4.

4.2 Sample Problem 2 - Center Cracked Plate

As illustrated in Figure 4-5, a center cracked plate with non-symmetric heat sources was analyzed as the second sample problem. The crack length in this problem is again assumed

to be 2 inches. Heat convection coefficients used are

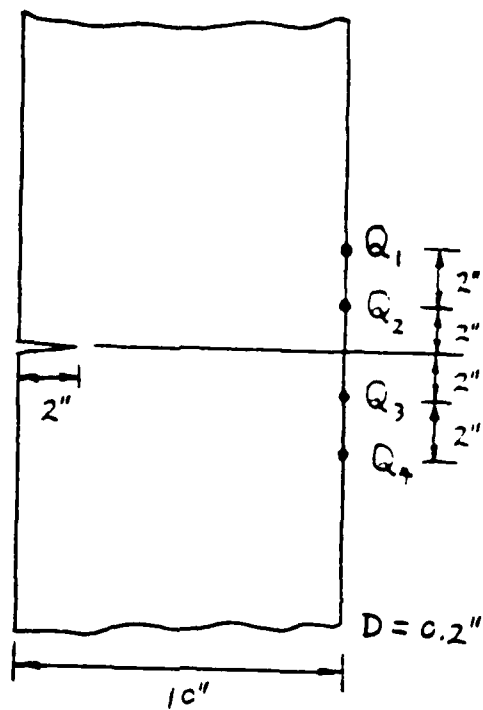
$$H_1 = H_2 = 0, \quad H = 0.0001929 \text{ Btu}/(\text{sec-F-in}^2)$$

and heat sources are applied at (2.5,2) and (7.5,-2) with

$$Q_1 = Q_2 = H(t-150) - H(t-1200) \quad \text{Btu}$$

As can be seen in Figure 4-5, this corresponds to loading points just above and below the crack plane, on alternating sides of the crack, and subject to the same transient load history defined above in sample problem 1.

Results of this sample problem are shown in Figures 4-6 through 4-8. Because of the non-symmetry, both normal and shear stresses develop at the crack plane, as illustrated in Figures 4-6A and B. The stress intensity factor shown in Figure 4-7, builds up and decays as before, but in this case both K_I and K_{II} are non-zero and are calculated directly by the program. Figure 4-8 shows the Green's functions at each crack tip (left and right) which result from the unit spike loading at heat source Q_1 .



$$Q_1 = Q_2 = Q_3 = Q_4 = Q(t)$$

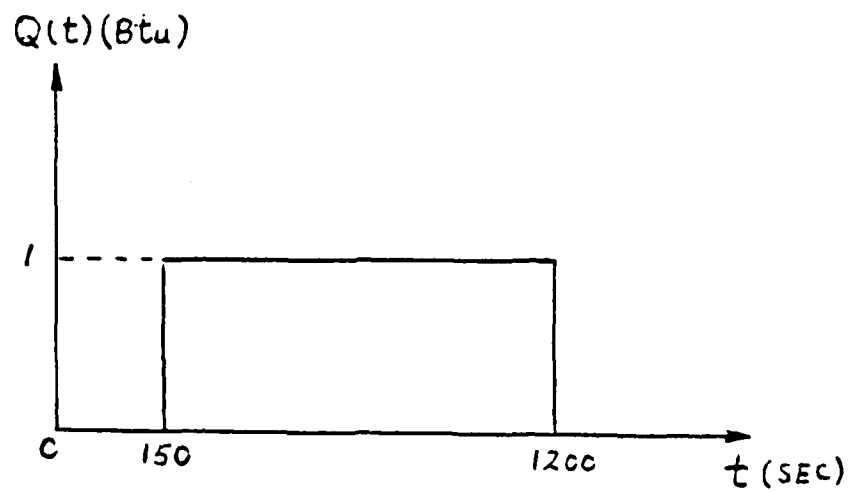


Figure 4-1. Sample Problem I

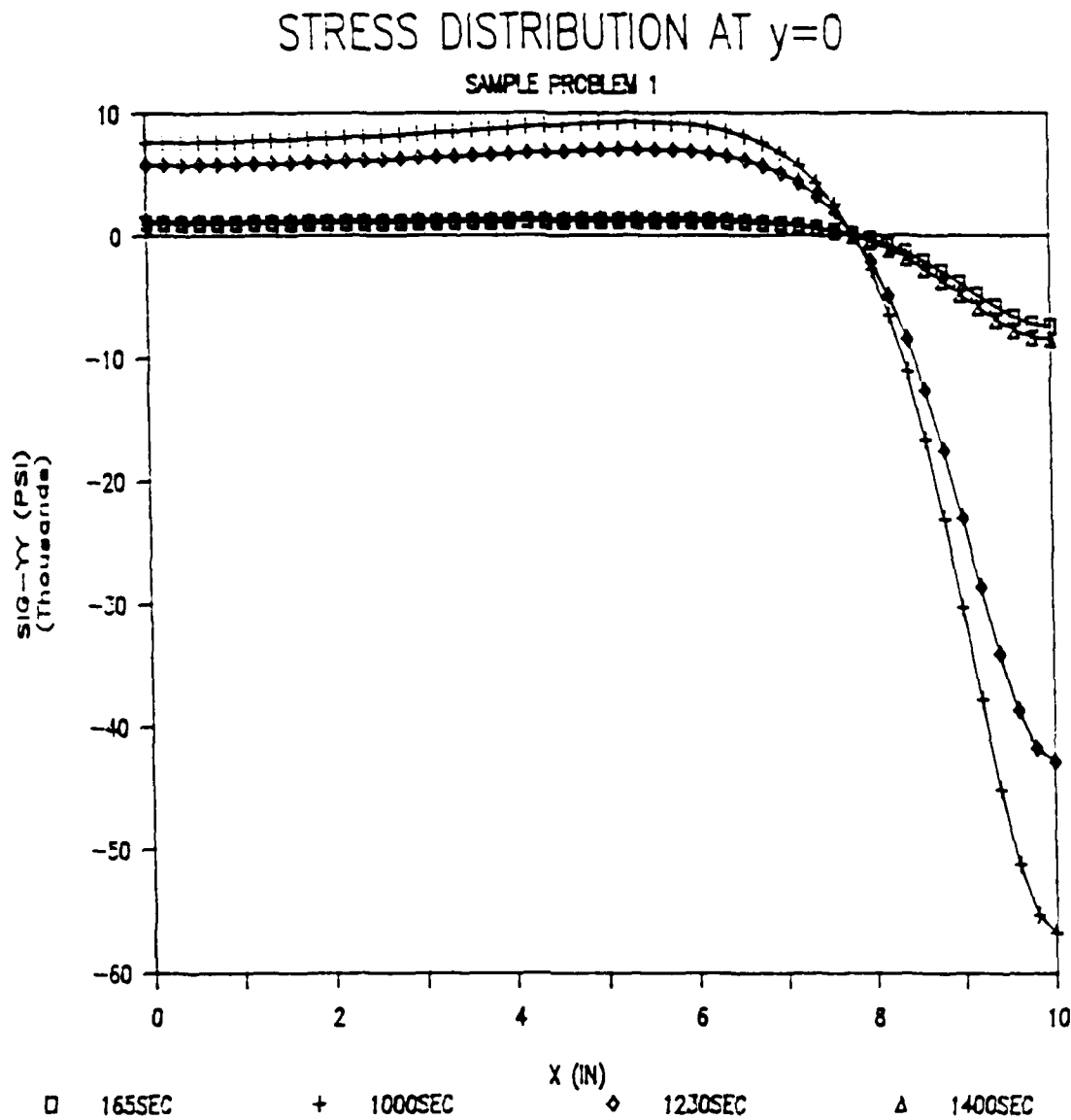


Figure 4-2. Stress Distribution at $y = 0$ for Sample Problem 1 ($\sigma_{xy} = 0$)

STRESS INTENSITY FACTORS

SAMPLE PROBLEM 1

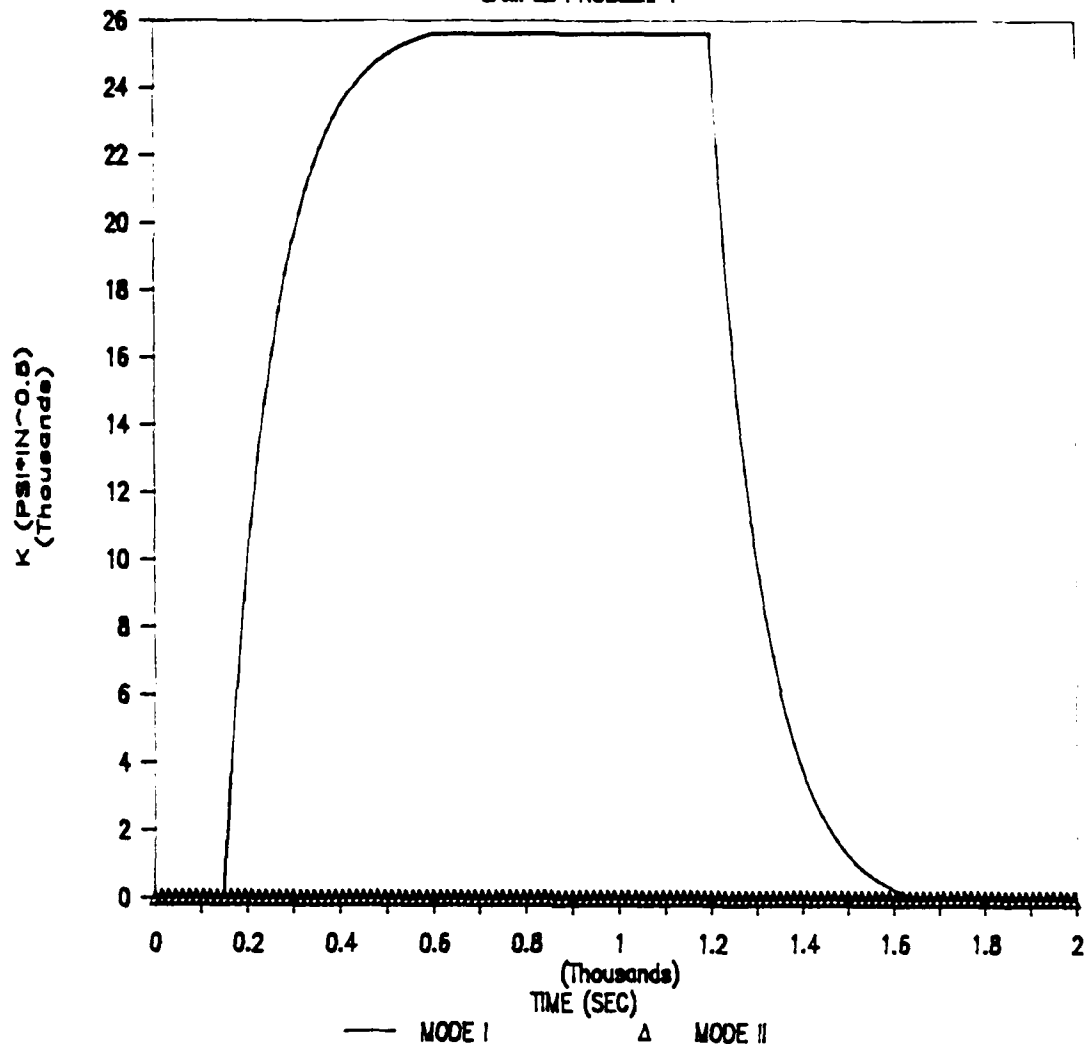


Figure 4-3. Stress Intensity Factors for Sample Problem 1

GREEN'S FUNCTIONS

SAMPLE PROBLEM 1

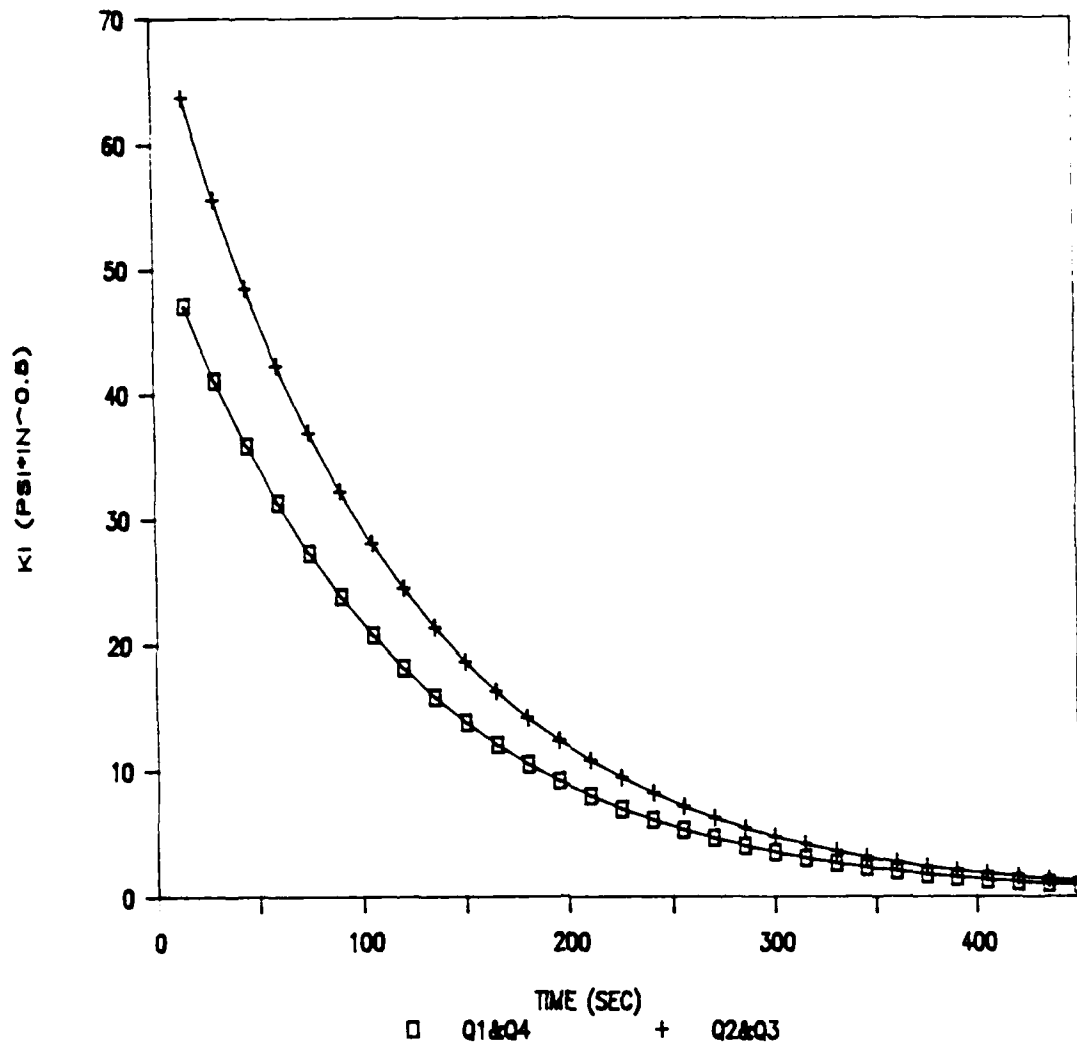
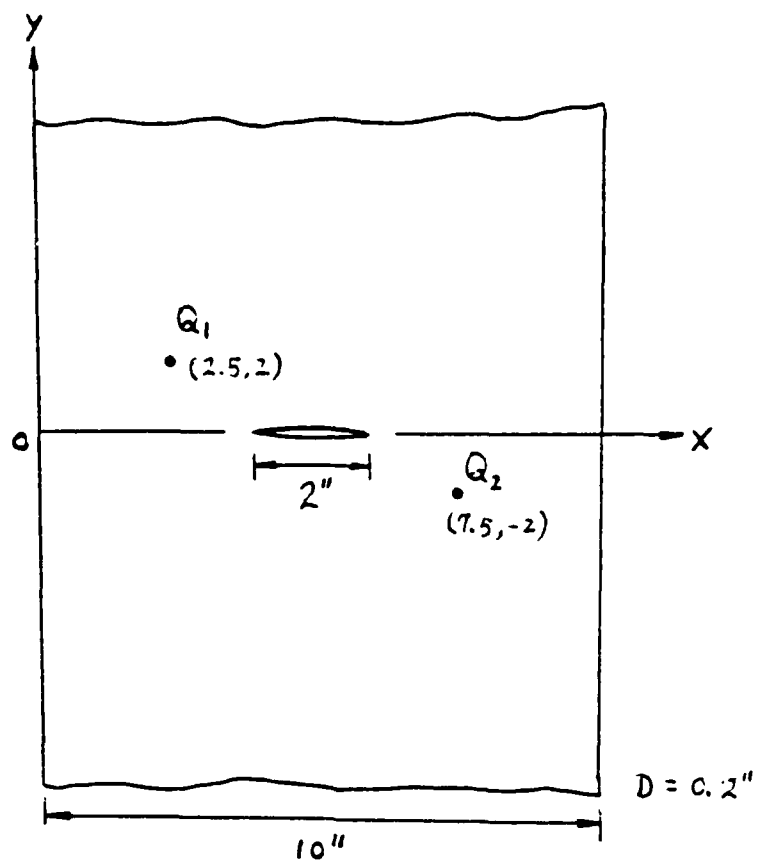


Figure 4-4. Green's Functions for Sample Problem 1
(Mode I only, Mode II = 0)



$$Q_1 = Q_2 = Q(t)$$

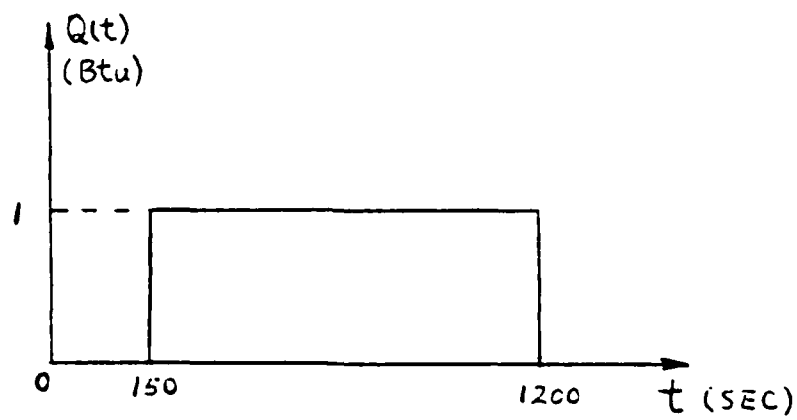


Figure 4-5. Sample Problem 2

STRESS DISTRIBUTION AT $y=0$

SAMPLE PROBLEM 2

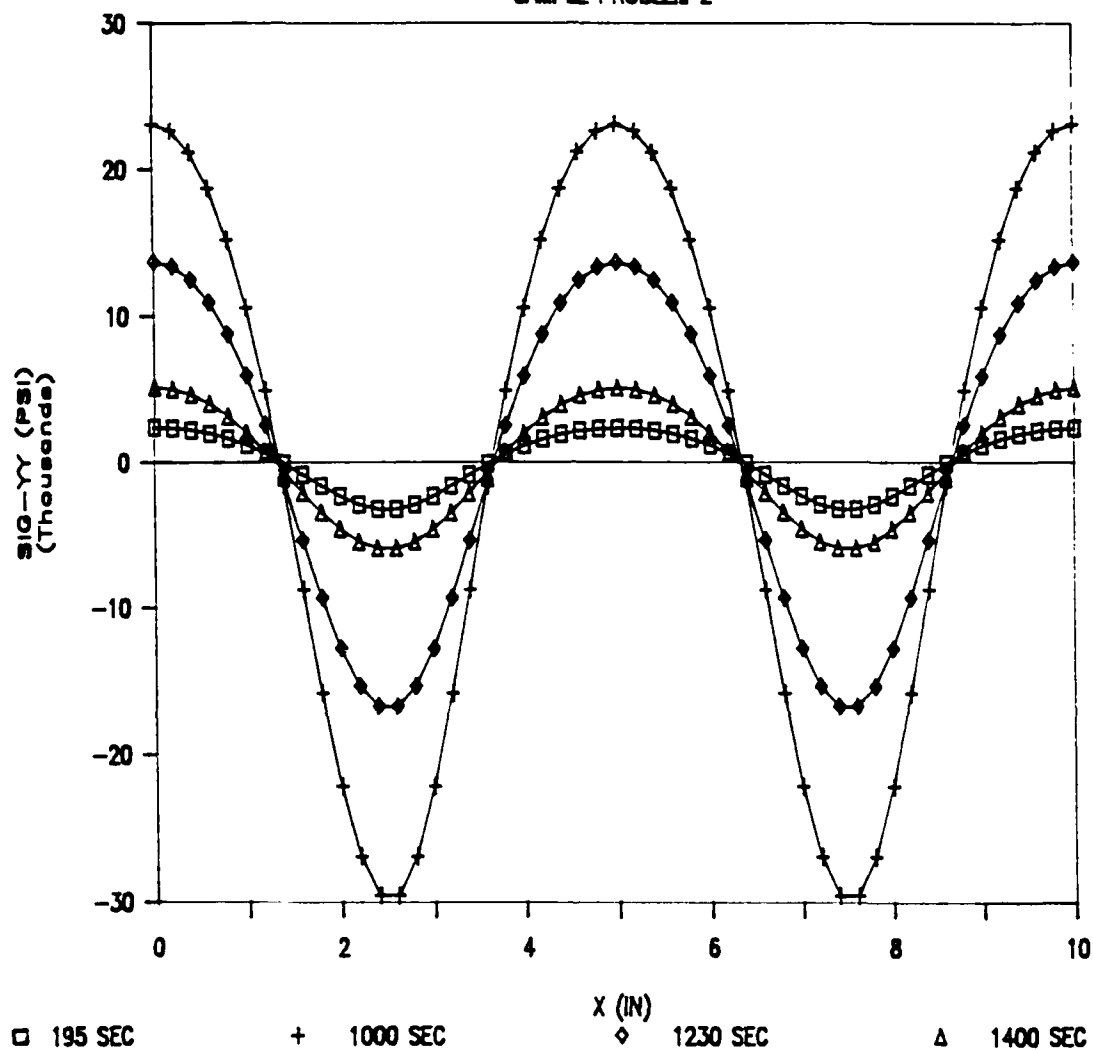


Figure 4-6A. Stress Distribution for Sample Problem 2 (σ_{yy})

STRESS DISTRIBUTION AT $y=0$

SAMPLE PROBLEM 2

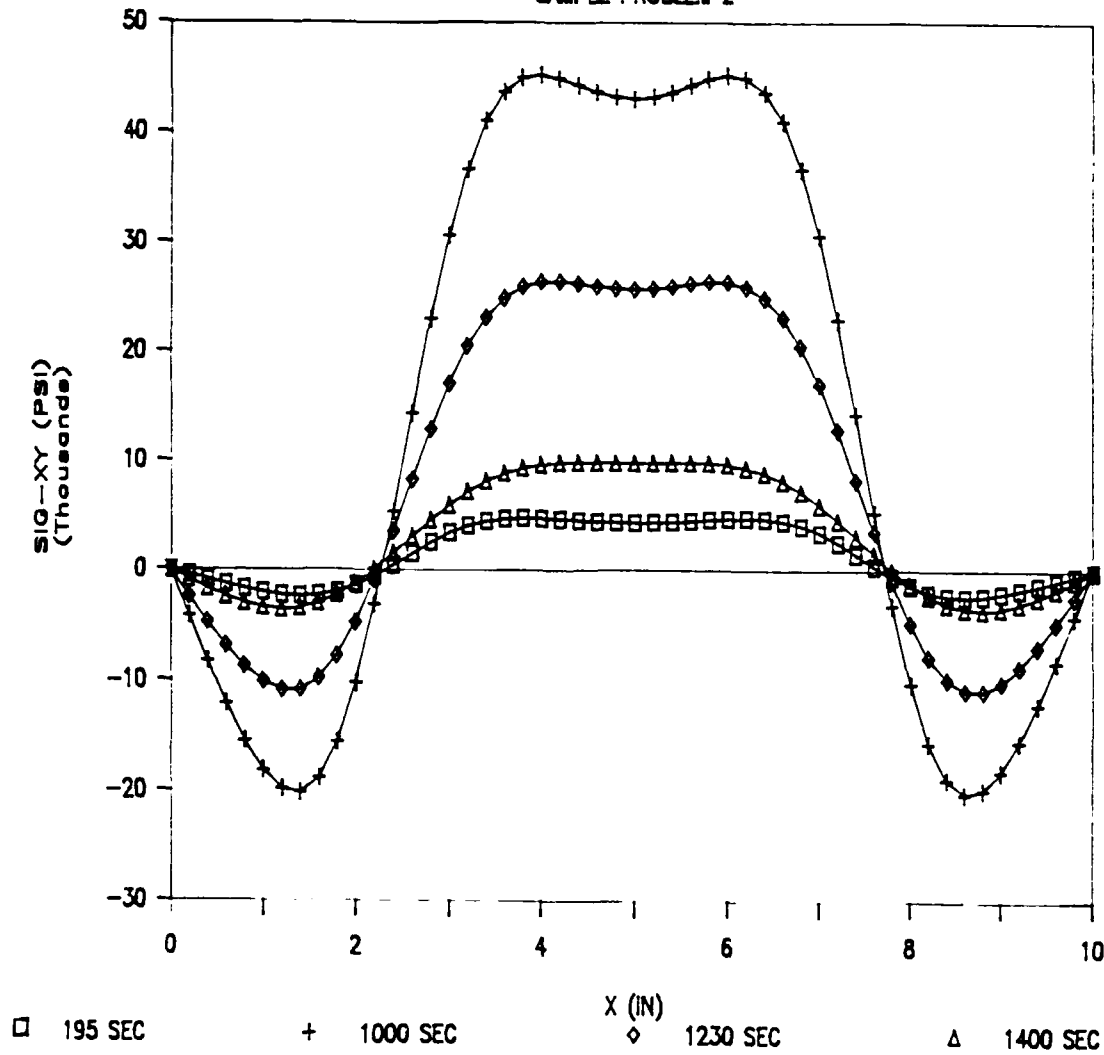


Figure 4-6B. Stress Distributions for Sample Problem 2 (σ_{xy})

STRESS INTENSITY FACTORS

SAMPLE PROBLEM 2 (BOTH CRACK TIPS)

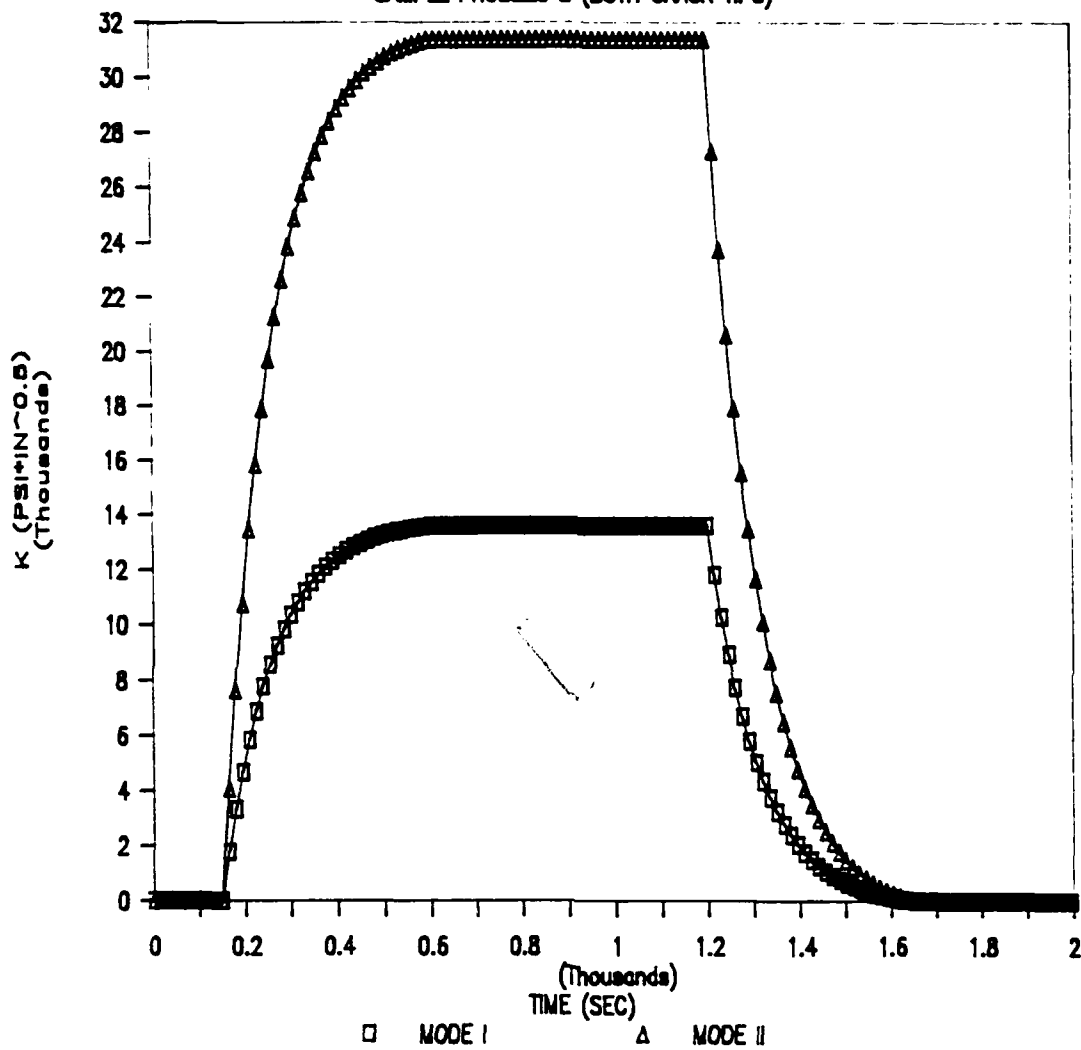


Figure 4-7. Stress Intensity Factors for Sample Problem 2
(the same curves for both crack tips)

GREEN'S FUNCTIONS FOR Q1 AT (7.5,-2)

SAMPLE PROBLEM 2

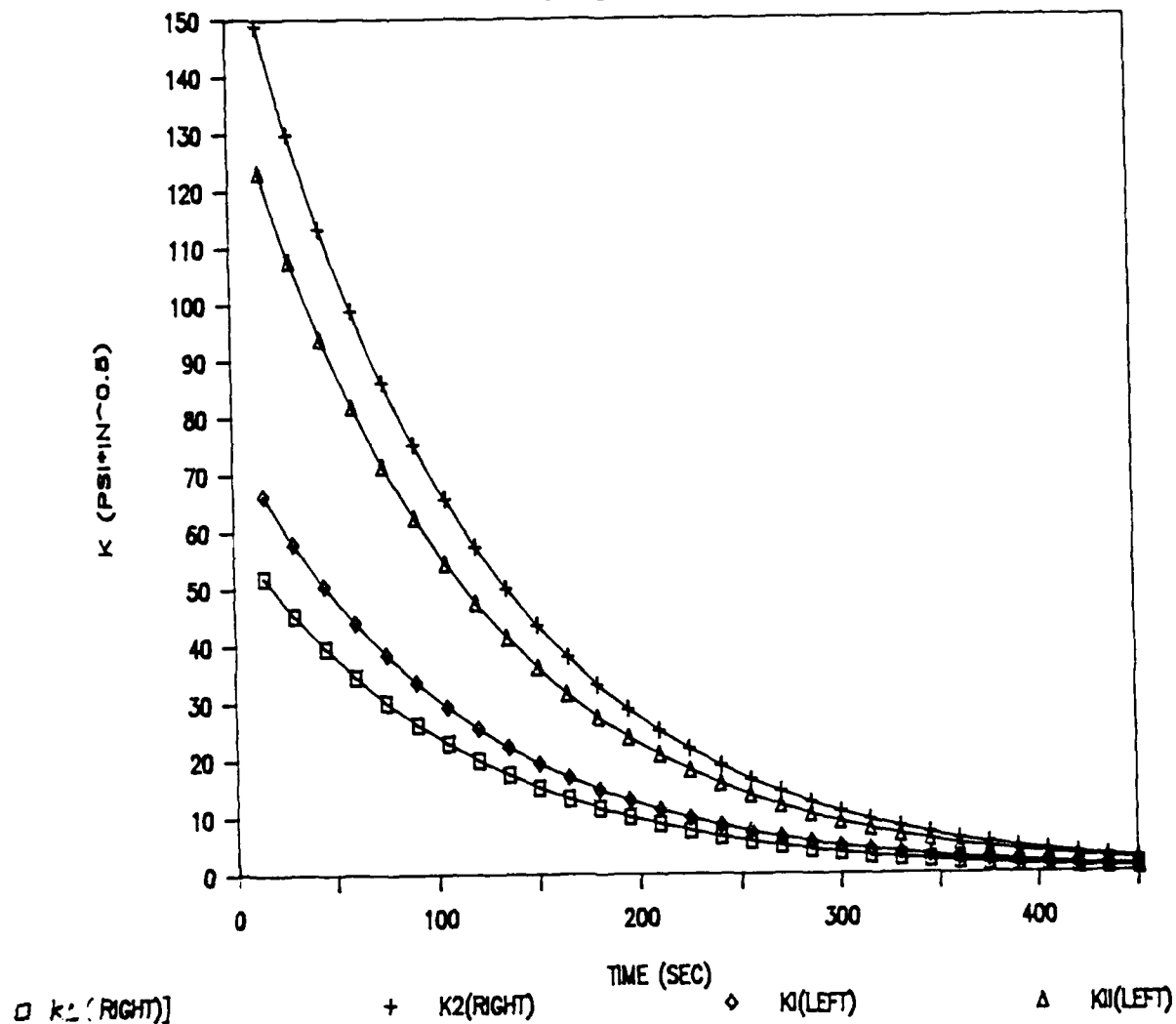


Figure 4-8. Green's Functions Due to Q1 for Sample Problem 2
(Q2 has similar curves)

5.0 CONCLUSIONS AND RECOMMENDATIONS

The Green's function concept derived in this report, coupled with the well-known use of influence functions for calculating stress intensity factors, is shown to provide a powerful tool for fracture mechanics analysis of cracked metallic structures under rapid thermal transients. Due to the nature of the Green's function decay characteristics, stress intensity factors for selected crack models can be easily calculated in a few minutes on an IBM-PC or compatible personal computer. Such a short turnaround time makes it possible to conduct thorough parametric studies for cracked structures subject to this type of loading, at a very low cost, both in terms of computer time and manpower, as compared to other means of problem solution known to the authors at this time. Also, using a novel software bus concept, the resulting computer program, AF-CRACK, is able to interface directly with the popular LOTUS-123 spreadsheet/graphics software package, which greatly enhances the graphics capability and ease of use of the program.

Through selected verification problems for which other solutions are available, the AF-CRACK program is shown to accurately predict stress and stress intensity factor, in comparison to other techniques. This preliminary verification, however, covered only a small portion of the general program capabilities, and further verification is recommended.

Based on the success of the Phase I feasibility study reported here, we concluded that it is highly feasible to develop a fast, accurate and easy to use general purpose computer program based on this methodology to predict stress

intensity factors for a wide range of metallic (or other) structures of interest to the Air Force, under rapid thermal pulses. It is also possible to connect the program with other fracture mechanics computer programs, to use the resulting stress intensity data in crack propagation or critical flaw size predictions.

Thus we recommend pursuing a Phase II effort to complete the program development effort begun by this study. The following areas have been identified as candidates for further study/development in the subsequent phases of the project:

(1) Provide more crack models. The basic methodology can be expanded applicable to a wide range of models, such as cracks emanating from a hole in a plate, cracks in cylindrical structures, and finite aspect ratio cracks (e.g. thumbnail surface cracks).

(2) Extend the program to mixed mode crack problems. In the preliminary version of AF-CRACK, only one of the two crack models has both mode I and mode II solutions. To be able to handle realistic problems, we must have the mixed mode solutions for all the crack models.

(3) Extend the Green's function solutions to problems in which the crack surfaces are insulated, because actual crack surfaces are expected to behave somewhere between fully heat conductant (as assumed here) and insulated. Conceptually, this type of Green's function can be derived by superimposing a continuous heat dipole along the crack surface onto the existing Green's function

(4) Study the limitations of the quasi-static thermoelasticity used in this study relative to planned

applications (heating rates) of the software. The two assumptions should be considered independently to determine separately at what heat rates the lack of inertia terms and the decoupling of the equations break down.

(5) If possible, and if the study of step (4) deems it to be desirable, include inertia effects into the existing, decoupled thermoelasticity equations for the Green's functions.

(6) Investigate the limitations of the linear elastic fracture mechanics theory used by the program relative to planned applications.

(7) Perform additional verification of the program both through additional comparisons with existing analytical solutions and through experiments.

(8) Furnish links between AF-CRACK and other fracture mechanics software designated by the Air Force. (eg. pc-CRACK, CRACKS-84 & -86, CRACKGRO, ASDGRO, etc.)

(9) Conduct parametric studies, using the software, of the effects of various heat sources and locations on stress intensity factors in structural configurations of interest to the Air Force. In addition to providing useful technical results, this will also provide feedback to the program developers on user friendliness, speed and convenience of the program in a typical application.

REFERENCES

1. LOTUS-123 - Release 2.01, Software and User's Manual, Lotus Development Corp., Cambridge, MA, 1986.
2. Bueckner, H. F., "Field Singularities and Related Integral Representations," in Methods of Analysis and Solutions of Crack Problems, Vol 1, ed. G. C. Sih, pp. 179-314, Noordhoff, Holland, 1973.
3. Tada, H., and Paris, P., and Irwin, G, The Stress Analysis of Cracks Handbook, Del Research Co., Pennsylvania, 1973.
4. Carslaw, H. S., and Jaeger, J. C., Conduction of Heat in Solids, 2nd edition, Oxford University Press, London, 1959.
5. Boley, B. A., and Weiner, J. H., Theory of Thermal Stresses, Wiley & Sons, New Yory, 1960.
6. Parkus, H., Thermoelasticity, Blaisdell Publishing Co., 1968.
7. Timoshenko, S. P., and Goodier, J. N., Theory of Elasticity, 3rd edition, McGraw Hill, New York, 1970.
8. TestPro - Computer Software for Ultrasonic Signal Analysis, User's Guide, Infometrics, Inc. (Subsidiary of Structural Integrity Associates), Silver Spring, MD, 1986.
9. pc-CRACK - Fracture Mechaanics Software for Personal Computers, Users Manual, Version 1.1, Revision 1, Structural Integrity Associates, San Jose, CA, June, 1986.
10. FEM2D - Two Dimensional Finite Element Computer Program for Heat Transfer/Thermal Stress Analysis, Users Manual, Structural Integrity Associates, San Jose, CA, March, 1986.
11. Abramowitz, M., and Stegun, I., Handbook of Mathematical Functions, Dover, New York, 1965.

APPENDIX A - INFLUENCE FUNCTIONS

A.1 Single Edge Cracked Plates

For a single edge crack in an infinite strip of plate, as illustrated in Figure 2-4, the influence function (or weight function) for mode I cracking has been provided by Bueckner [2] as

$$m_1(x) = \frac{1}{\sqrt{a-x}} \left[1 + p_1 \left(\frac{a-x}{a} \right) + p_2 \left(\frac{a-x}{a} \right)^2 \right] \quad (A1)$$

where

$$p_1 = 0.6147 + 17.1844 R^2 + 8.8722 R^6 \quad (A2)$$

$$p_3 = 0.2502 + 3.2889 R^2 + 70.0444 R^6 \quad (A3)$$

$$R = a/B \quad (A4)$$

and x , a , and B are defined in Figure 2-4.

Bueckner [2] has stated that the above equations for the weight function $m_1(x)$ are very accurate for cracks up to half of the plate width, B . The authors cannot find the

corresponding influence function $m_2(x)$ for the mode II cracks after a preliminary literature survey. However, we felt that the solution for $m_2(x)$ might already exist or can be obtained numerically by finite element analyses in the following phase of this project.

A.2 Center Cracked Plates

Influence functions for a center crack in an infinite strip of plate, as illustrated in Figure 2-5, have been derived by Tada, et al. [3] as follows

$$m_1(x) = m_2(x) = \frac{1}{\sqrt{2B}} \{F_1[\frac{a}{B}, (\frac{x}{a} - \frac{1}{2})]\} \{F_2[\frac{a}{B}, (\frac{x}{a} - \frac{1}{2})]\} \quad (A5)$$

where

$$F_1(\xi, \eta) = 1 + 0.297 \sqrt{(1 - \eta^2)} (1 - \cos \frac{\pi}{2} \xi) \quad (A6)$$

$$F_2(\xi, \eta) = \sqrt{\tan \frac{\pi}{2} \xi} \frac{1 \pm (\sin \frac{\pi}{2} \eta / \sin \frac{\pi}{2} \xi)}{\sqrt{1 - (\cos \frac{\pi}{2} \xi / \cos \frac{\pi}{2} \eta)^2}} \quad (A7)$$

and x , a , and B are defined in Figure 2-5. In equation (A7) the plus sign is for the right crack tip and the minus sign is for the left crack tip.

Tada [3] shows that equations (A6) and (A7) are accurate within 1% for all crack sizes.

APPENDIX B - SOLUTION FOR COMPLEMENTARY STRESS FUNCTION ψ

This Appendix discusses the solution procedure for the stress function ψ and its resulting stress $\hat{\sigma}_{yy}$ and $\hat{\sigma}_{xy}$ in equations (28-36).

It has been discussed by Timoshenko [7] that the solution for the problem illustrated in Figure 2-7 can be written as

$$\begin{aligned} \psi = & \frac{1}{\pi} \int_0^{\infty} (C_1 \cosh \beta \bar{x} + C_2 \sinh \beta \bar{x} + C_3 \bar{x} \cosh \beta \bar{x} + C_4 \bar{x} \sinh \beta \bar{x}) \cos \beta y \, d\beta \\ & + \frac{1}{\pi} \int_0^{\infty} (D_1 \cosh \beta \bar{x} + D_2 \sinh \beta \bar{x} + D_3 \bar{x} \cosh \beta \bar{x} + D_4 \bar{x} \sinh \beta \bar{x}) \sin \beta y \, d\beta \end{aligned} \quad (B1)$$

where $\bar{x} = x - (B/2)$. In equation (B1), the eight constants C_1 , C_2 , ..., D_3 , and D_4 are determined by the boundary conditions at $x=0$ and $x=B$. As explained in equations (32 through 34), the boundary conditions for ψ at the two edges, $x=0$ and $x=B$, are the non-zero stresses due to stress function ϕ of equation (25). By substituting equations (25 through 27) into equations (33 and 34), the boundary conditions for ψ can be written as follows

at $x=0$ ($\bar{x} = -B/2$),

$$\psi_{,yy} = F_1(y) \quad (B2)$$

$$\psi_{,xy} = F_2(Y) \quad (B3)$$

and at $x=B$ ($\bar{x}=B/2$),

$$\psi_{,yy} = F_3(Y) \quad (B4)$$

$$\psi_{,xy} = F_4(Y) \quad (B5)$$

where

$$\begin{aligned} F_1(Y) = & - \frac{\alpha(1+\nu)Q}{4\rho cD} \sum Z_n(0) Z_n(x') \{ \\ & \exp(\alpha_n(y-y')) [\alpha_n \operatorname{erfc}(\omega_1) + 2 \frac{\exp(-\omega_1^2)}{\sqrt{\pi \xi t}} - \frac{\omega_1 \exp(-\omega_1^2)}{\sqrt{\pi} \alpha_n \xi t}] \\ & + \exp(-\alpha_n(y-y')) [\alpha_n \operatorname{erfc}(\omega_2) + 2 \frac{\exp(-\omega_2^2)}{\sqrt{\pi \xi t}} - \frac{\omega_2 \exp(-\omega_2^2)}{\sqrt{\pi} \alpha_n \xi t}] \} \end{aligned} \quad (B6)$$

$$\begin{aligned} F_2(Y) = & \frac{\alpha(1+\nu)Q}{4\rho cD} \sum Z'_n(0) Z_n(x') \{ \\ & \exp(\alpha_n(y-y')) [\operatorname{erfc}(\omega_1) + \frac{\exp(-\omega_1^2)}{\sqrt{\pi \xi t} \alpha_n}] \\ & - \exp(-\alpha_n(y-y')) [\operatorname{erfc}(\omega_2) + \frac{\exp(-\omega_2^2)}{\sqrt{\pi \xi t} \alpha_n}] \} \end{aligned} \quad (B7)$$

$$F_3(Y) = - \frac{\alpha(1+\nu)Q}{4\rho cD} \sum Z_n(B) Z_n(x') \{$$

$$\begin{aligned}
& \exp(\alpha_n(y-y')) \left[\alpha_n \operatorname{erfc}(\omega_1) + 2 \frac{\exp(-\omega_1^2)}{\sqrt{\pi \xi t}} - \frac{\omega_1 \exp(-\omega_1^2)}{\sqrt{\pi} \alpha_n \xi t} \right] \\
& + \exp(-\alpha_n(y-y')) \left[\alpha_n \operatorname{erfc}(\omega_2) + 2 \frac{\exp(-\omega_2^2)}{\sqrt{\pi \xi t}} - \frac{\omega_2 \exp(-\omega_2^2)}{\sqrt{\pi} \alpha_n \xi t} \right] \} \\
& \hspace{15em} (B8)
\end{aligned}$$

$$\begin{aligned}
F_4(y) &= \frac{\alpha(1+\nu)Q}{4\rho cD} \sum Z'_n(B) Z_n(x') \{ \\
& \exp(\alpha_n(y-y')) \left[-\operatorname{erfc}(\omega_1) - \frac{\exp(-\omega_1^2)}{\sqrt{\pi \xi t} \alpha_n} \right] \\
& - \exp(-\alpha_n(y-y')) \left[\operatorname{erfc}(\omega_2) + \frac{\exp(-\omega_2^2)}{\sqrt{\pi \xi t} \alpha_n} \right] \} \\
& \hspace{15em} (B9)
\end{aligned}$$

After solving the eight constants, C_1, C_2, \dots, D_3 , and D_4 , the stresses at $y=0$, can be expressed in a double integration as follows

$$\begin{aligned}
\hat{\sigma}_{yy} &= -\frac{2G}{\pi} \int_{-\infty}^{\infty} \int_0^{\infty} \{ [\beta^2 (R_1 \cosh \beta \bar{x} + R_2 \sinh \beta \bar{x} + R_3 \bar{x} \cosh \beta \bar{x} \\
& + R_4 \bar{x} \sinh \beta \bar{x}) F_1(y)] + [\beta^2 (-R_1 \cosh \beta \bar{x} + R_2 \sinh \beta \bar{x} \\
& + R_3 \bar{x} \cosh \beta \bar{x} - R_4 \bar{x} \sinh \beta \bar{x}) F_3(y)] \} \cos \beta y \, d\beta \, dy \\
& - \frac{2G}{\pi} \int_{-\infty}^{\infty} \int_0^{\infty} \{ [\beta^2 (V_1 \cosh \beta \bar{x} + V_2 \sinh \beta \bar{x} + V_3 \bar{x} \cosh \beta \bar{x} \\
& + V_4 \bar{x} \sinh \beta \bar{x})] [F_2(y) + F_4(y)] \} \sin \beta y \, d\beta \, dy \quad (B10)
\end{aligned}$$

$$\begin{aligned}
\hat{\sigma}_{xy} = & -\frac{2G}{\pi} \int_{-\infty}^{\infty} \int_0^{\infty} \{ [(V_1\beta \sinh\beta\bar{x} + V_2\beta \cosh\beta\bar{x} + V_3(\cosh\beta\bar{x} \\
& + \beta\bar{x} \sinh\beta\bar{x}) + V_4(\sinh\beta\bar{x} + \beta\bar{x} \cosh\beta\bar{x})] \\
& [F_3(y)+F_4(y)] \} \beta \sin\beta y \, d\beta \, dy \\
& -\frac{2G}{\pi} \int_{-\infty}^{\infty} \int_0^{\infty} \{ [(R_1\beta \sinh\beta\bar{x} + R_2\beta \cosh\beta\bar{x} \\
& + R_3(\cosh\beta\bar{x} + \beta\bar{x} \sinh\beta\bar{x}) + R_4(\sinh\beta\bar{x} + \beta\bar{x} \cosh\beta\bar{x})] F_1(y) \\
& + [-R_1\beta \sinh\beta\bar{x} + R_2\beta \cosh\beta\bar{x} + R_3(\cosh\beta\bar{x} + \beta\bar{x} \sinh\beta\bar{x}) \\
& - R_4(\sinh\beta\bar{x} + \beta\bar{x} \cosh\beta\bar{x})] F_3(y) \} \beta \sin\beta y \, d\beta \, dy \quad (B11)
\end{aligned}$$

where

$$R_1 = \frac{1}{\beta^2} [\sinh(\frac{\beta B}{2}) + (\frac{\beta B}{2}) \cosh(\frac{\beta B}{2})] / (\beta B + \sinh\beta B) \quad (B12)$$

$$R_2 = \frac{1}{\beta^2} [\cosh(\frac{\beta B}{2}) + (\frac{\beta B}{2}) \sinh(\frac{\beta B}{2})] / (\beta B - \sinh\beta B) \quad (B13)$$

$$R_3 = -[\frac{1}{\beta} \cosh(\frac{\beta B}{2})] / (\beta B - \sinh\beta B) \quad (B14)$$

$$R_4 = -[\frac{1}{\beta} \sinh(\frac{\beta B}{2})] / (\beta B + \sinh\beta B) \quad (B15)$$

$$V_1 = -[\frac{B}{2\beta} \sinh(\frac{\beta B}{2})] / (\beta B + \sinh\beta B) \quad (B16)$$

$$V_2 = \left[\frac{B}{2\beta} \cosh\left(\frac{\beta B}{2}\right) \right] / (\beta B - \sinh\beta B) \quad (B17)$$

$$V_3 = - \left[\frac{1}{\beta} \sinh\left(\frac{\beta B}{2}\right) \right] / (\beta B - \sinh\beta B) \quad (B18)$$

$$V_4 = \left[\frac{1}{\beta} \cosh\left(\frac{\beta B}{2}\right) \right] / (\beta B + \sinh\beta B) \quad (B19)$$

In numerical calculation, the integration in equations (B10) and (B11) can be evaluated by using the Gauss-Laguerre quadrature and Gauss-Hermite quadrature [11]. In AF-CRACK, six points were used for the Gauss-Laguerre quadrature, and five points are used for the Gauss-Hermite quadrature. That is, the integration can be carried out approximately by

$$\int_0^{\infty} F(z) dz = \sum W_i F(z_i) \exp(z_i) \quad (B20)$$

where

$$z_1 = 0.222846604179 \quad , \quad W_1 = 0.458964673950$$

$$z_2 = 1.188932101673 \quad , \quad W_2 = 0.417000830772$$

$$z_3 = 2.992736326059 \quad , \quad W_3 = 0.113373382074$$

$$z_4 = 5.775143569105 \quad , \quad W_4 = 0.103991974531 \times 10^{-1}$$

$$z_5 = 9.837467418383 \quad , \quad W_5 = 0.261017202815 \times 10^{-3}$$

$$z_6 = 15.982873980602 \quad , \quad W_6 = 0.898547906430 \times 10^{-6}$$

and by

$$\int_{-\infty}^{\infty} F(z) dz = \sum W_i F(z_i) \exp(z_i^2) \quad (\text{B21})$$

$$z_{1,5} = \pm 2.0201828705 \quad , \quad W_{1,5} = 0.0199532421$$

$$z_{2,4} = \pm 0.9585724646 \quad , \quad W_{2,4} = 0.3936193232$$

$$z_3 = 0.0 \quad , \quad W_3 = 0.9453087205$$

APPENDIX C - PATH INDEPENDENT LINE INTEGRALS
FOR STEADY-STATE, TWO-DIMENSIONAL THERMOELASTICITY

ABSTRACT

Three path-independent line integrals J'_k , M' , and L'_3 are derived for the steady-state, two-dimensional thermoelasticity. These integrals are similar to the J_k , M , and L_3 presented by Knowles and Sternberg [1], but include additional terms of either free expansion displacement vector u_k^* or temperature θ and its complex conjugate $\bar{\theta}$ in their formulation. These new line integrals enable us to avoid the undesirable area integration [2] when calculating the strain energy release rate for crack problems. Application of J'_k , M' , and L'_3 is demonstrated through a sample problem of a constant heat flux disturbed by a finite crack in an infinite plate.

1.0 INTRODUCTION

Since the discovery of the conservation integrals J_k , M , and L by Knowles and Sternberg [1], several similar conservation integrals have been introduced for the thermoelasticity. Gurtin [3] has proposed a line integral which consists of, in addition to the well-known J_1 -integral, three more terms related to the temperature field. Unfortunately, path-independence of the line integral proposed by Gurtin relies on several restrictions which in general can not be met, e.g., one of the restrictions is that the temperature distribution has to be symmetric about the crack axis and equal to zero on the crack surfaces. Aoki, et al. [2] have derived another set of path independent integrals \hat{J}_k , \hat{M} , \hat{L} , and \hat{I} for general elastic-plastic problems. As a special case for the two-dimensional thermoelasticity, these integrals become

$$\hat{J}_k = \int_{\Gamma} (W n_k - T_j u_{j,k}) ds - \int_A \sigma_{mj} \delta_{mj} \alpha_1 \theta dA \quad (C1)$$

$$\hat{M} = \int_{\Gamma} (W n_j - T_k u_{k,j}) x_j ds - \int_A \sigma_{jk} \delta_{jk} \alpha_1 (\theta, x_m + \theta) dA \quad (C2)$$

$$\begin{aligned} \hat{L}_3 = & \int_{\Gamma} e_{j3k} (W n_j - T_m u_{m,j}) x_k + T_j u_k ds \\ & - \int_A e_{j3k} \alpha_1 (2\sigma_{km} \delta_{jm} \theta + \sigma_{pq} \delta_{pq} \theta, x_k) dA \end{aligned} \quad (C3)$$

where j, k, m, p , and $q = 1$ or 2 , W is strain energy density, α_1 is equivalent coefficient of thermal expansion defined in (C14), θ is temperature distribution, Γ is a intergration contour enclosing the crack tip, A is the area bounded by Γ , and e_{ijk} is an alternate tensor. Although the above three integrals are path-independent, addition of the extra area integration at the end of (C1), (C2), and (C3) have ruined one of the merits of the path-independent integrals. For isothermal elastostatic problems, the three line integrals, J_k , M , and L introduced by Knowles and Sternberg [1] allow us to take advantage of its path-independence and calculate the energy release rate based on solutions far away from the singular crack tip. However, when calculating the energy release rate by (C1), (C2), or (C3), a highly accurate stress and temperature solution near the crack tip is necessary in order to evaluate the area integration accurately, implying higher computer cost and potential arguments on how accurate is enough for the solution near the crack tip.

For the steady-state, two-dimensional thermoelasticity, the present study eliminates the need of area integrations by introducing three path-independent line integrals J'_k , M' , and L'_3 .

2.0 FORMULATION

2.1 Governing Equations

Consider a plane strain or plane stress deformation field under a steady state temperature distribution. It is assumed that no body force or distributed heat source are present. Governing equations for the steady-state, two-dimensional thermoelasticity problem are

$$\sigma_{jk,k} = 0 \quad \text{in } B \quad (C4)$$

$$\sigma_{jk} = \delta_{jk} \lambda \epsilon_{mm} + 2\mu \epsilon_{jk} - \delta_{jk} (3\lambda + 2\mu) \alpha \theta \quad (C5)$$

$$\epsilon_{jk} = (u_{j,k} + u_{k,j})/2 \quad (C6)$$

$$\sigma_{jk} n_k = T_j^0 \quad \text{on } S_\sigma \quad (C7)$$

$$u_j = u_j^0 \quad \text{on } S_u \quad (C8)$$

$$\theta_{,jj} = 0 \quad \text{in } B \quad (C9)$$

$$\theta = \theta^0 \quad \text{on } S_T \quad (C10)$$

$$\theta_{,n} = Q \quad \text{on } S_Q \quad (C11)$$

where summation convention has been implicitly used for repeated subscripts with $j, k = 1, 2$, B is the elastic body with S as its boundary, S_σ , S_u , S_T , and S_Q are subsets of the boundary S , n is the normal direction of S , α is coefficient of thermal expansion, and λ and μ are Lamé's elastic constants defined by

$$\lambda = \frac{E_1 \nu_1}{1 - \nu_1^2}, \quad \mu = \frac{E_1}{2(1 + \nu_1)} \quad (C12)$$

in which $E_1 = E$ and $\nu_1 = \nu$ for plane stress problems, and $E_1 = E/(1 - \nu^2)$, and $\nu_1 = \nu/(1 - \nu)$ for plane strain problems (E and ν are Young's modulus and Poisson's ratio respectively).

2.2 Conservation Laws

As a start, let us assume that the elastic body B is simply connected. Extension of the formulation to multiply connected bodies is discussed in 2.4. The area integrations in (C1) through (C3) can be converted into line integrations by introducing a new variable Ω , which is a complex conjugate function of θ , into the formulation. θ and Ω are thus related by the Cauchy-Riemann equations

$$\theta_{,1} = \Omega_{,2}, \quad \text{and} \quad \theta_{,2} = -\Omega_{,1} \quad (C13)$$

Let us define another new variable u_j^* , the free expansion displacement, as

$$u_1^* + iu_2^* = \alpha_1 \int (\theta + i\Omega) dz \quad (C14)$$

where $z = x_1 + ix_2$ and $\alpha_1 = \alpha$ for plane stress problems or $\alpha_1 = (1 + \nu)\alpha$ for plane strain problems. With (C13) and (C14), the area integration in (C1) can be rewritten as

$$\int_A \sigma_{jm} \delta_{jm} \alpha_1 \theta_{,k} dA = \int_A \sigma_{jm} u_{j,mk}^* dA = \int_\Gamma \sigma_{jm} n_m u_{j,k}^* ds \quad (C15)$$

where

$$u_{1,1}^* = u_{2,2}^* = \alpha_1 \theta, \quad u_{1,2}^* = -u_{2,1}^* = -\alpha_1 \Omega \quad (C16)$$

Thus (C1) becomes

$$J'_k = \int_{\Gamma} [W n_k - T_j u'_{j,k}] ds \quad (C17)$$

where

$$u'_j = u_j - u_j^*, \quad (C18)$$

or

$$J'_1 = \int_{\Gamma} \{W n_1 - T_j u_{j,1} + \alpha_1 (T_1 \theta + T_2 \Omega)\} ds \quad (C19)$$

and

$$J'_2 = \int_{\Gamma} \{W n_2 - T_j u_{j,2} - \alpha_1 (T_1 \Omega - T_2 \theta)\} ds \quad (C20)$$

Similarly, (C2) and (C3) can be rewritten as

$$M' = \int_{\Gamma} (W n_j - T_k u'_{k,j}) x_j ds \quad (C21)$$

or

$$M' = \int_{\Gamma} \{ (W n_j - T_k u_{k,j}) x_j + \alpha_1 \theta (T_1 x_1 + T_2 x_2) - \alpha_1 \Omega (T_1 x_2 - T_2 x_1) \} ds \quad (C22)$$

and

$$L'_3 = \int_{\Gamma} e_{j3k} \{ (W n_j - T_m u'_{m,j}) x_k + T_j u'_{j,k} \} ds \quad (C23)$$

L'_3 can not be expressed in terms of θ and Ω like (C19), (C20), and (C22) because the last term in the integrand of (C23) would

result terms involving $\int (\theta + i\Omega) dz$. Thus, for the steady-state, two-dimensional thermoelasticity, the conservation integrals defined in (C1), (C2), and (C3) can be reduced to line integrals with the addition of u_j^* or θ and Ω in their formulation. We see from (C17), (C21), and (C23) that, with u_j^* being the parts of the displacement, formulations of J_k' , M' , and L_3' for the thermoelasticity are identical to formulation of J_k , M , and L_3 for the isothermal elasticity. This observation is similar to the analogy between the governing equations for the thermoelasticity and isothermal elasticity discussed in [4].

One way to calculate J_k' , M' , or L_3' is to solve for Ω , in addition to the original heat transfer/thermal stress problem, and use (C19), (C20) or (C21). Since Ω is the complex conjugate of θ , it satisfies the Laplace equation and can be solved in closed form or numerically with a set of boundary conditions conjugate to that for θ . Another words, Ω is the solution of

$$\Omega_{,jj} = 0 \quad \text{in } B \quad (C24)$$

$$\Omega_{,n} = 0 \quad \text{on } S_T \quad (C25)$$

and

$$\Omega_{,s} = -Q \quad \text{on } S_Q \quad (C26)$$

where n and s are normal and tangential directions respectively of the boundary S . Alternatively, J_k' , M' , and L_3' can be calculated by solving for the free expansion displacement u_j^* and substituting them into (C17), (C21), or (C23).

2.3 Free Expansion Displacement u_j^*

The free expansion displacement u_j^* introduced in (C14) is not only for the convenience of formulation but also physically meaningful. Substitution of (C16) and (C6) into (C5) yields

$$\sigma_{jk} = \delta_{jk} \lambda (u_{j,j}^! + u_{k,k}^!) + \mu (u_{j,k}^! + u_{k,j}^!) \quad (C27)$$

where $u_j^!$ is defined by (C18). By the definition of $u_j^!$, it is easy to deduce that, when $u_j = u_j^*$, all displacement, stress, and strain components vanish. Therefore, u_j^* is the stress free displacement for the elastic body under the same temperature θ as the original problem. For a simply connected body, u_j^* is the displacement solution for the same body B under the same temperature distribution θ but with homogeneous mechanical boundary conditions, i.e. $T_1=0$ and no prescribed displacements on the boundary. It is worth noting that, although all the stress components corresponding to u_j^* in the x_1 - x_2 plane are zero, the stress component σ_{33} associated with u_j^* will, in general, not be zero for plane strain problems.

2.4 Multiply Connected Body

Since most of the elastic bodies we deal with in fracture problems are multiply connected, it is important to extend $J_K^!$, $M^!$, and $L_j^!$ to multiply connected bodies. For an $(m+1)$ -ply connected body, Ω and u_j^* are still the complex conjugate of θ and the stress free displacement field with homogeneous mechanical boundary conditions, respectively. But, when solving for Ω and u_j^* , m additional cuts have to be introduced to make the body simply connected. Surfaces of these m cuts are stress free and can move freely against each other, i.e. overlapping or sliding

of the two adjacent faces on each cut are permitted for u_j^* . Also, $\Omega_{,n}$ is continuous across the cuts with n being the normal direction of the cuts. The additional m cuts are necessary because, for a multiply connected body, Ω and u_j^* may be multi-valued even though its counter part θ is still singled-valued [4]. In general, Ω and u_j^* are not continuous across the cuts, in a multiply connected body, therefore, formulations for J'_k , M' , and L'_j must be modified to account for the discontinuities when the integration contour Γ intersects any of the cuts. For instance, for contour Γ_1 in Figure 1, an additional term of

$$\int_{C_1} T_j[u_{j,k}^*] ds \quad (C28)$$

$$\int_{C_1} T_j[u_{j,k}^*] x_k ds \quad (C29)$$

and

$$-\int_{C_1} e_{3mj} (T_m[u_j^*] - T_k[u_{k,m}^*] x_j) ds \quad (C30)$$

must be added to (C17), (C21), and (C23) respectively, where $[f]$ is the discontinuity of f across C_1 . Nevertheless, it is always possible to chose the cuts and the integration contours Γ in such a way that they do not intersect each other, e.g. contour Γ_2 in Figure 1. In this case, expressions in (C17) to (C23) are still valid for multiply connected bodies and the addition of (C28), (C29) or (C30) to the conservation integrals can be avoided. Finally, when solving for Ω and u_j^* , selection of the m cuts to make an $(m+1)$ -ply connected body simply connected is not unique, neither are the solutions for Ω and u_j^* , but the final values of

J'_k , M' , and L'_3 do not depend on the choice of the cuts or the integration contours.

2.5 Energy Release Rates and Stress Intensity Factors

Similar to the physical interpretation of J_k , M , and L_3 in the isothermal elasticity [5], J'_k , M' , and L'_3 defined in (C17) to (C23) can be deemed as the energy release rates associated with translation, rotation, and self-similar expansion of the crack, respectively. Moreover, since the order of stress singularity at the crack tip for the two dimensional thermoelasticity is still $-1/2$ [6], the relationships between energy release rates and stress intensity factors for the isothermal plane elasticity [5,7,8] also apply to the thermoelasticity problems, i.e.

$$J'_1 = (K_I^2 + K_{II}^2)/E_1 \quad (C31)$$

and

$$M' = x_1^0 J'_1 \quad (C32)$$

where E_1 is defined in section 2.1 and x_1^0 is the x_1 -coordinate of the crack tip in a Cartesian coordinate system of which x_1 -axis is along the crack surface.

3.0 EXAMPLE PROBLEM

To study the effectiveness of J'_k , M' , and L'_3 in numerical calculation, an example problem of a finite crack of length $2a$ in an infinite plate with prescribed temperature gradient $v\theta$ at infinity is chosen. The temperature gradient $v\theta$ at infinity is assumed to be perpendicular to the crack. Stress intensity factor for this problem has been found [6] to be

$$K_{II} = (2\mu\alpha a\sqrt{\pi a} \nabla\theta)/(1+\kappa) \quad (C33)$$

where μ is shear modulus, α is coefficient of thermal expansion, and κ equals to $(3-4\nu)$ for plane strain problems or $(3-\nu)/(1+\nu)$ for plane stress problems.

A finite element program with built-in J_1' routine is used to solve this problem. As shown in Figure C-2, a finite size rectangular plate is used to simulate the infinite plate. Due to the inherent symmetry of the problem, only one half of the plate is needed in the finite element analysis. A total of 249 nodes and 70 eight-node isoparametric elements is used. We found after a few numerical experiments that numerical solution to this problem is not sensitive to the size of the finite plate once the length on each side of the finite plate is more than ten times of the crack length. Also shown in Figure C-2 are five integration contours to calculate J_1' . A standard heat transfer/thermal stress analysis is first performed for this problem followed by another analysis for either Ω or u_j^* so that J_1' can be calculated at the five selected contours based on (C17) or (C20). For this doubly connected body, a cut along A-B in Figure C-2 is introduced when solving for Ω and u_j^* . Since there is no intersection between the cut A-B and the five integration contours, (C17) and (C20) can be used without modification. Boundary conditions for the finite element analyses are summarized in Table C-1. Once J_1' is calculated, the stress intensity factor can be determined by (C31).

Resulting stress intensity factors based on two different equations, (C17) and (C21) are listed and compared with the exact solution (C33) in Table C-2. It is seen from this table that stress intensity factors predicted by J_1' and finite element methods are essentially path independent except for the first contour. Larger errors at the first contour is expectable since

the finite element mesh at the crack tip is relatively coarse, and stress distributions near the crack tip are thus not expected to be highly accurate. However, with only 249 nodal points and 70 elements in the finite element model, stress intensity factors calculated based on J_1' at the other four contours are within 5% or 3%, depending upon whether (C17) or (C21) is used, of the exact solution given by Sih [6]. Judging by numerical accuracy and computational cost, formulations of J_k' , M' , and L_3' in terms of θ and Ω , (C19), (C20) and (C22), is preferable to those in terms of u_j^* , (C17), (C21) and (C23). However, formulations of J_k' , M' , and L_3' in terms of u_j^* still provide a good alternative when Ω is difficult to obtain.

4.0 CONCLUSION

Conservation integrals for thermoelasticity have been found to contain extra area integration terms which often make these path-independent integrals less attractive compared to other methods, such as special crack-tip elements. However, for plane strain or plane stress problems under steady state temperature distributions, such a undesirable area integration can be eliminated by using one of the three path-independent line integrals, J_k' , M' , and L_3' , introduced in this paper. To use J_k' , M' , or L_3' , an auxiliary variable, u_j^* or Ω , has to be solved in addition to θ and u_j of the original problem. Solution to the auxiliary problem of u_j^* or Ω can be obtained numerically or in closed form without much difficulty. Physically, Ω is a complex conjugate of the temperature distribution θ and u_j^* are the stress free displacements. It has been shown in this paper through an example problem that the energy release rates or stress intensity factors for cracks in a two dimensional solid under steady state temperature can be easily calculated with J_1' or M' and a relatively coarse finite element model.

5.0 REFERENCES

1. J. K. Knowles and E. Sternberg, *Archive for Rational Mechanics Analysis* 44 (1972) 187-211.
2. S. Aoki, K. Kishimoto, and M. Sakata, *Journal of Applied Mechanics* 48 (1981) 825-829.
3. M. E. Gurtin, *International Journal of Fracture* 15 (1979) R169-R170.
4. N. I. Muskhelishvili, "Some Basic Problems of Mathematical Theory of Elasticity," 4th Ed., Noordoff, Groningen (1963).
5. B. Budianski, and J. R. Rice, *Journal of Applied Mechanics* 40 (1973) 201-203.
6. G. C. Sih, *Journal of Applied Mechanics* 29 (1962) 587-589.
7. L. B. Freund, *International Journal of Solids and Structures* 14 (1978) 241-250.
8. A. G. Hermann and G. Hermann, *Journal of Applied Mechanics* 48 (1981) 525-528.

Table C-1
Summary of Boundary Conditions

	for u_j	for u_j^*	for θ	for Ω
A-B	$u_1=0$	$T_j=0$	$\theta_{,1}=0$	$\Omega=0$
B-O-C	$T_j=0$	$T_j=0$	$\theta_{,2}=0$	$\Omega=0$
C-D	$u_1=0$	$u_1=0$	$\theta_{,1}=0$	$\Omega=0$
D-E	$T_j=0$	$T_j=0$	$\theta_{,2}=-\nabla\theta$	$\Omega_{,2}=0$
E-F	$T_j=0$	$T_j=0$	$\theta_{,1}=0$	$\Omega_{,1}=\nabla\theta$
F-A	$T_j=0$	$T_j=0$	$\theta_{,2}=-\nabla\theta$	$\Omega_{,2}=0$

Table C-2

Normalized Stress Intensity Factor $\frac{(1+\kappa) K_{II}}{2\mu\alpha a\sqrt{\pi a} \sqrt{\theta}}$

	with (2.11)	with (2.13)
contour 1	1.133	1.184
contour 2	0.951	0.974
contour 3	0.955	0.977
contour 4	0.952	0.975
contour 5	0.952	0.970
Sih [6]	1.000	1.000

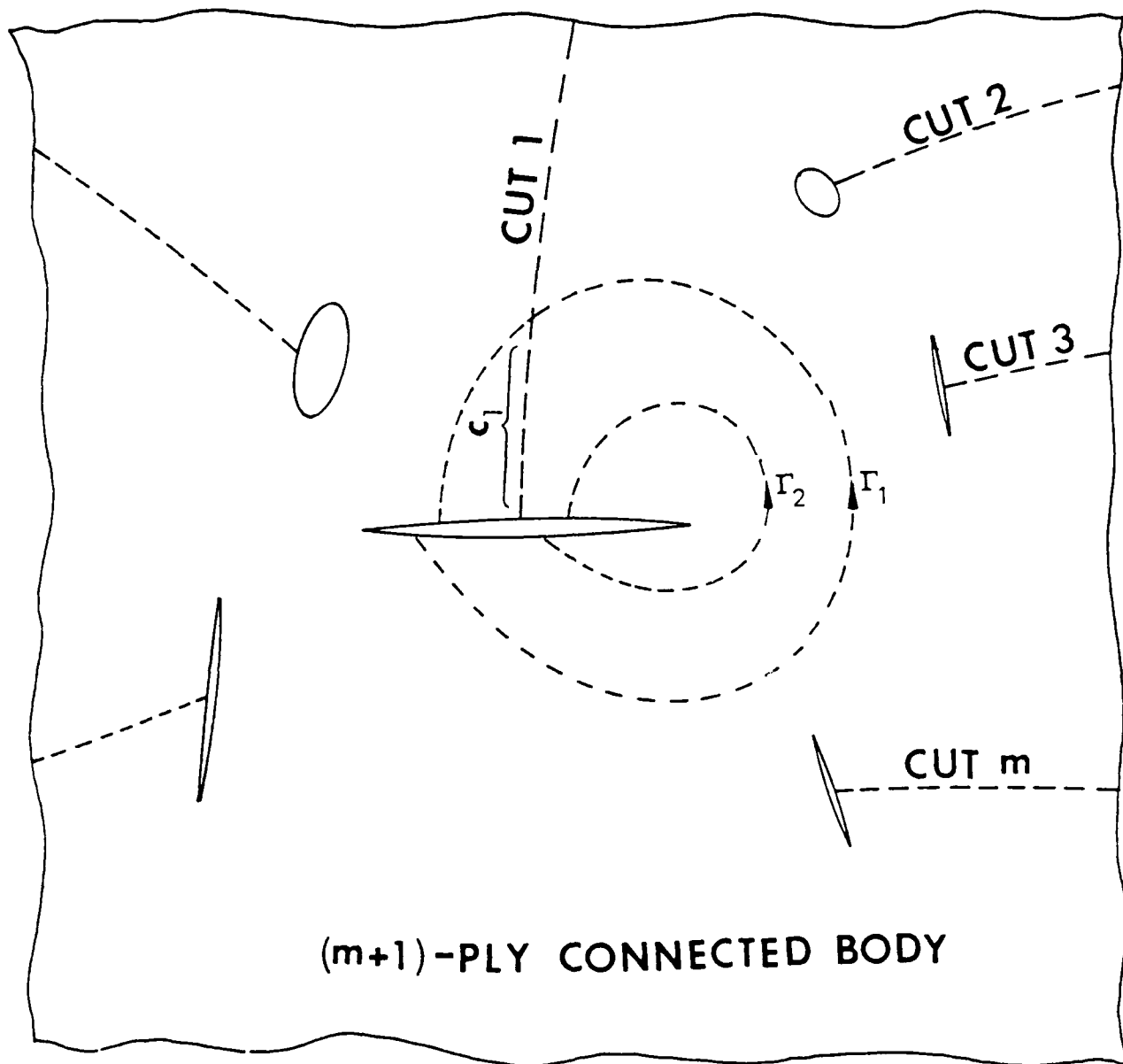


Figure C-1 $(M+1)$ -ply Connected Body with m Cuts

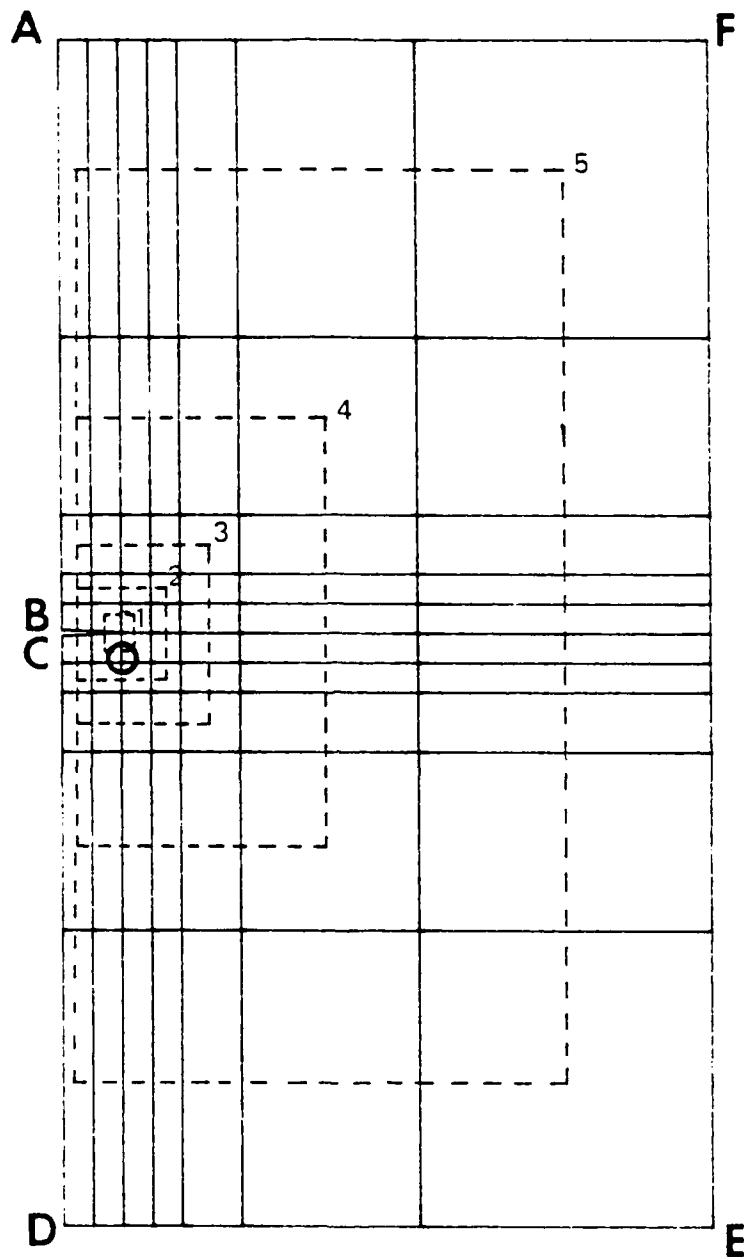


Figure C-2 Finite Element Model